# MODELLING FLOW THROUGH POROUS MEDIA UNDER LARGE PRESSURE GRADIENTS

A Dissertation

by

SHRIRAM SRINIVASAN

Submitted to the Office of Graduate and Professional Studies of
Texas A&M University
in partial fulfillment of the requirements for the degree of

DOCTOR OF PHILOSOPHY

| | |
|---|---|
| Chair of Committee, | Kumbakonam Rajagopal |
| Committee Members, | Andrea Bonito |
| | Robert Handler |
| | Anastasia Muliana |
| | Jay Walton |
| Head of Department, | Andreas A. Polycarpou |

December 2013

Major Subject: Mechanical Engineering

ABSTRACT

The most interesting and technologically important problems in the study of flow through porous media involve very high pressures and pressure gradients in the flow domain such as enhanced oil recovery and carbon dioxide sequestration. The popular Darcy or Brinkman models do not take into account the changes in the fluid properties (like viscosity) due to high pressures and temperatures, or the deformation of the solid itself as the fluid flows through it. We focus on the pressure dependence of viscosity and show that its significance in these problems cannot be neglected.

Mixture theory is employed as the tool to develop models for this task. The popular models due to Darcy and Brinkman (and their generalizations) are derived using a general thermodynamic framework which appeals to the criterion of maximal rate of entropy production. Such a thermodynamic approach has been used with great success to describe various classes of material response and here we demonstrate its use within the context of mixture theory. One such generalization of the Brinkman model takes into account the variation of the viscosity and the drag coefficient with the pressure and is used in the problems studied subsequently.

We then consider the steady flow of a fluid through a porous slab, driven by a large pressure gradient, and show that the traditional approach that ignores the variation of the viscosity and drag with the pressure greatly over-predicts the mass flux taking place through the porous structure. While incorporating the pressure dependence of viscosity and drag leads to a ceiling flux, the traditional approaches lead to a continued increase in the flux with the pressure difference.

The effect of inhomogeneities and anisotropy of the porous medium is investigated by modifying the previous problem to prescribe the drag coefficient as a piecewise constant, positive definite second order tensor. Finally, we allow for the possibility that the flow is unsteady, the viscosity and drag are dependent on the pressure and consider the flow of a

fluid due to a pulsatile forcing pressure at one end of a rigid, homogenoues, isotropic solid while the other end is open to the atmosphere. In contrast to certain non-Newtonian fluids where the volumetric flux is enhanced by pulsating the pressure gradient about a non-zero mean value, we find that pulsations in the pressure diminish the volumetric flux in case of the flow through a porous medium when the fluid viscosity is considered to be pressure dependent.

DEDICATION

My Captain does not answer, his lips are pale and still;
My father does not feel my arm, he has no pulse nor will;
The ship is anchor'd safe and sound, its voyage closed and done;
From fearful trip, the victor ship, comes in with object won;
Exult, O shores, and ring, O bells!
But I, with mournful tread,
Walk the deck my Captain lies,
Fallen cold and dead.

– *Walt Whitman*

ACKNOWLEDGEMENTS

It is my pleasure to write this section of my dissertation with feelings as warm, buoyant and sanguine as when I wrote the corresponding section of my Master's thesis. That it is so despite the interlude of a few years is due in large part to the people I shall mention presently. I intend the remark to be a compliment when I say that lack of discontent with my life has perhaps led me to finish my program of study somewhat later than I would have anticipated.

My advisor, Professor K.R.Rajagopal has supervised my progress as a student with the rare quality of giving precedence to understanding and knowledge over outcomes and results, and afforded me the opportunity to pursue what I term an "old fashioned" Ph.D., something I shall always cherish. The necessity of acute awareness of the fundamental definitions and tacit assumptions inherent in any subject or theory is a lesson so deeply ingrained, I would like to think that oversight of this point is unlikely to be one of my failings, numerous as they may otherwise be. Working with him has been an enriching experience and I thank him for the opportunity; if and when I eventually get the opportunity to advise students, his influence on my thoughts will be unmistakable.

Professors Arun Srinivasa and Natarajan Sivakumar are two other remarkable people who have had an enormous influence on me.

My interest in the subject of continuum mechanics was kindled in the first graduate course taught by Prof. Srinivasa. Since then, I have endeavoured to get his insights on teaching, research, and sundry matters, for conversation with him is an inspiration and an absolute pleasure. I earnestly hope that I can continue to learn and benefit from his magnanimity.

It is to Prof. Sivakumar that I owe my gratitude for giving me the confidence and knowledge to embark on the path to getting a Master's degree in Mathematics, and serving as my committee chair for the degree. His patience has never worn thin, even with questions

that could be fairly deemed asinine. I consider myself fortunate to have had the benefit of his wit, counsel and company.

I could not have done any better for myself during my stay in Texas A&M than to have found good reason to engage with these three gentlemen in various capacities. Their words and actions have been unanimous in their message that admittance of ignorance is not infra dig.

I also thank Professors Andrea Bonito, Robert Handler, Anastasia Muliana and Jay Walton for serving on the committee.

I am pleased to acknowledge my friends and colleagues, fellow students who served as sounding boards, discussions with whom have contributed in part to my knowledge of things (Matlab, LaTeX, Linux, Mathematics, Mechanics, Python) which I devoted most of my time to: (in no particular order) Messrs. Keaton Hamm, Karthik Sundar, Jayavel Arumugam, Sudarshan Parthasarathy, Spencer Patty, Alagappan Ponnalagu, Fahad Alrashed, Ashwin Rao, Mukundan Ragavan, Srikrishna Doraiswamy, Harsha Nagarajan, Drs. Atul Narayan, Saradhi Koneru and Pritha Ghosh, and Misses. Anjana Talapatra and Fatma Terzioglu.

Many thanks to Mukundan Ragavan; the time spent watching cricket and trouble shooting issues with my laptop are memorable, and indelible from memory is the morning of April 2, 2011.

I recollect with delight my association with Abhilasha Katariya, Anjana Talapatra and Pritha Ghosh.

Anjana Talapatra has an ability I prize highly, but alas lack in comparison; the ability to strip away the extraneous and squarely address the fundamental questions on matters of ethics and moral conduct. She has been a harsh critic and a great support for me during challenging times, giving me the confidence to follow the path I chose. She values the things that deserve to be valued and I am glad to have met her.

Finally, I would like to acknowledge my parents, who first inculcated in me a respect for scholarship and have always advised me to act to make myself happy, and my sister Lakshmi, for being herself.

TABLE OF CONTENTS

LIST OF FIGURES

FIGURE Page

LIST OF TABLES

TABLE Page

# 1. INTRODUCTION

## 1.1 Motivation

It is natural to imagine that when a flowing fluid encounters a solid object like a rock, part of the flow is arrested and the fluid flows past the object; that the rock is "impermeable" or "impervious" is an obvious assumption to make. The term "impermeable" is understood to mean "preventing especially liquids to pass through". A cursory glance through a thesaurus shows some of its synonyms to be "impervious","non-porous", "impassable", "watertight" etc. Familiarity with any one of these words is enough to expect that "impermeability" is an ideal, not likely to be attained in practice. One can also be convinced likewise by directing a sufficiently powerful microscope onto the surface of whatever object is believed to be impermeable and observe the surface maculated with pores.

Porous materials are ubiquitous. Objects in nature such as rocks, minerals and soil, biological tissues like skin, bones, membranes and wood, and man-made materials such as cements, ceramics and polymers are all instances of a porous medium. The study of fluid flow through porous media arises naturally and it has emerged as a separate field of study; the interaction between the fluid and the medium through which it flows adding a complexity absent in the study of deformable bodies.

One can characterize a porous medium by its *permeability*, *porosity*, and *saturation*.

**Porosity** is the fraction of the volume occupied by pores, and is a number between 0 to 1. It determines the amount of fluid the medium can hold.

**Saturation** is the fraction of the pore volume filled with fluid, and is a number between 0 to 1. A value of 1 indicates the medium is *saturated*, and the pores cannot hold any more fluid. We shall deal only with saturated porous media in this work, and hence no more will be said about it.

**Permeability** is a measure of the ability of a fluid to flow through a medium. It has

dimension $[L]^2$ and depends solely on the medium. As an example, the permeability of sand is $10^{-12}\,\mathrm{m}^2$ to $10^{-10}\,\mathrm{m}^2$ while for clay it is $10^{-17}\,\mathrm{m}^2$ to $10^{-15}\,\mathrm{m}^2$.

What then, is one to make of the phrase, "impermeable/impervious solid" ? The answer is that the term has more to do with one's perception of the object than something intrinsic to the object itself. To explain, without putting too fine a point on it, an object can be described as impermeable if in the time scale of observation, a negligible quantity of fluid flows through it. When a water body drains in clayey soil, observed over months or years, the permeability of clay cannot be neglected, but one stores water in a clay-pot without fear of leakage, and it is certainly reasonable to consider the clay-pot to be impermeable. The point just made lies at the heart of modelling and will be emphasized whenever an assumption is made about some aspect of the response of a body. As long as the assumption made does not contradict observations in real physical situations, it is reasonable to do so.

The study of flow through porous media finds context and relevance in a multitude of instances like filtration, soil and rock mechanics, movement of groundwater and contaminants in soils, flow of oil through a reservoir, diffusion of fluids through synthetic polymers and biological materials etc. The most interesting and technologically important problems of flow through porous media concern flows of fluids involving very high pressures and pressure gradients in the flow domain, with concomitant deformation of the porous medium. Examples of such applications are the problems of enhanced oil recovery and carbon dioxide sequestration, brief descriptions of which now follow.

### *1.1.1 Enhanced oil recovery (EOR)*

Traditional primary and secondary methods of oil recovery typically recover only one third of oil in place, leaving two thirds behind. During the life of a well, there is always a point at which the cost of producing an additional barrel of oil is higher than the price the market will pay for that barrel. Production then halts. In the past, the well used to be abandoned, even with 70 % of the oil left in the ground, since oil was easy to find and the economics dictated that it was cheaper to find and produce oil in a new field. However, things started to change when the declining reserves and the low probability of locating

significant new fields drove producers to seek additional oil in old reservoirs, making North America a proving ground for EOR techniques. EOR is also referred to as tertiary or improved oil recovery. Today, it is estimated that North America accounts for more than half the worlds EOR production [1].

EOR is an imprecise term used to describe an assortment of techniques that are used to recover oil once the primary and secondary recovery methods fail. The various techniques used in oil recovery are listed in Figure 1.1. The principle behind EOR is however the same in all methods; a fluid is injected into the injection wells at high pressure and it pushes the oil to the surface at the production well. The injection pressures involved are usually in excess of 600 atm [2]. Using EOR techniques up to an additional 30 % of oil may be recovered from the well. A typical EOR process in Weyburn oil field in Saskatchewan is depicted in Figure 1.2.

Thus, in the field of petroleum engineering, accurate estimate of oil production rate and economic feasibility of EOR hinge on the ability to model the physical process of oil recovery. However, this is no easy task due to a plethora of complications:

1. More than one fluid is involved. The flow could be multi-component/multi-phase in the sense that we could have a mixture of carbon dioxide, water, steam and oil.

2. The medium (soil) may deform and eventually fracture due to the high pressure of fluid flowing through it.

3. There could be various interaction mechanisms between the fluid and the solid.

4. The material properties of the fluid like viscosity and density could change due to the high pressures and elevated temperatures. The fluid could shear-thin or shear-thicken.

5. The medium may be heterogeneous, with strata of solid rock interspersed with clay or sand; hence the pore structure of the solid may not be uniform. If the solid is anisotropic, the permeability to flow may not be the same in all directions.

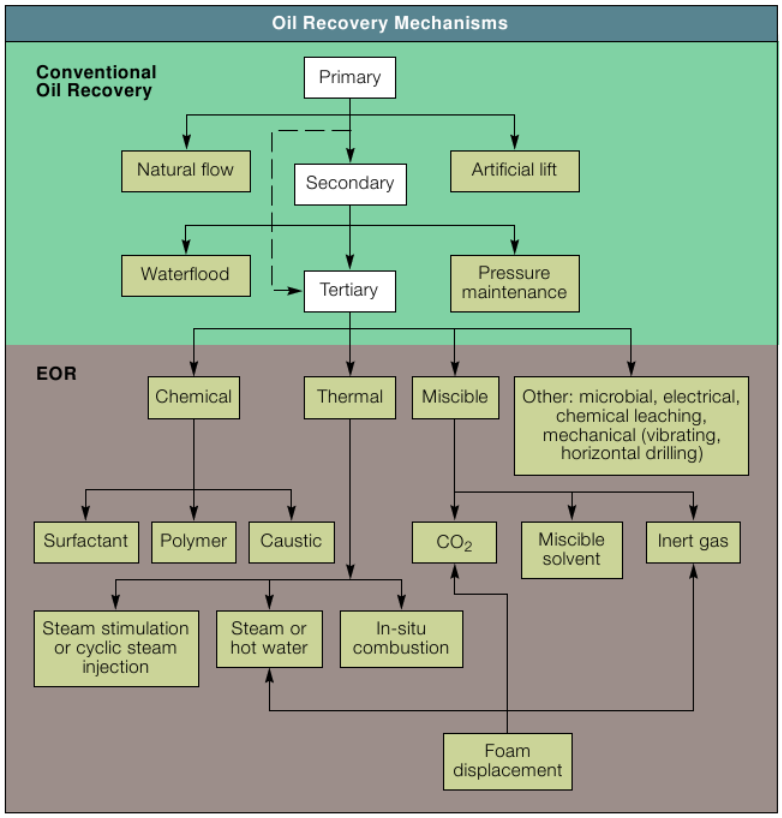


Figure 1.1: Methods of EOR (Source: Lake and Venuto [1])

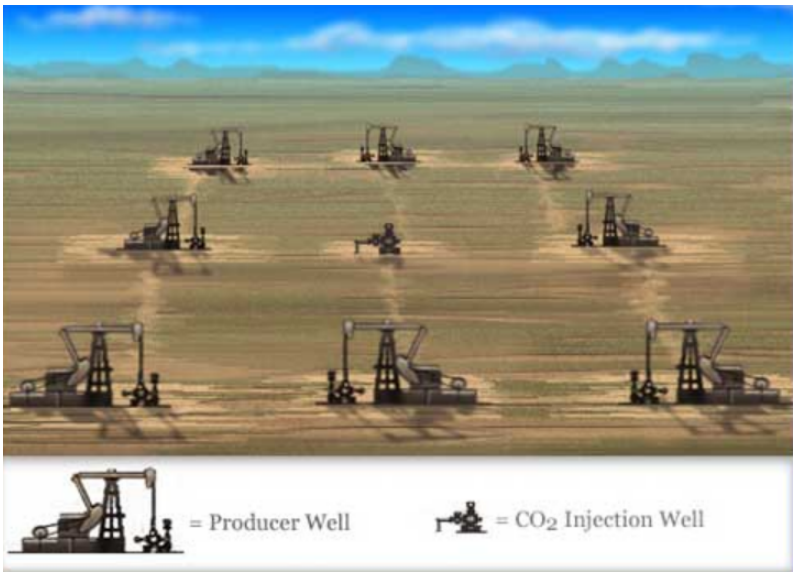


Figure 1.2: EOR setup (Source: `http://www.planetseed.com/node/15251`)

### *1.1.2 Carbon dioxide sequestration (CS)*

The techniques of EOR developed over the past few decades have now found another avenue for gainful employment: the engineering problem of carbon dioxide sequestration or geological sequestration. In this process, supercritical carbon-dioxide is pumped at high pressures into deep saline aquifers or abandoned oil wells and the pressure can vary from 1 atm to 500 atm [3]. This method has been proposed to reduce the level of atmospheric $CO_2$, since the increased level of the gas is suspected to contribute to global warming and adversely impact the climate. The idea of sequestering carbon dioxide to reduce the amount entering the atmosphere is fairly new. But the technology needed to do this has been developed for EOR already.

Thermal power stations, iron and steel plants and cement production plants are good candidates for capture and storage because they are large scale sources with a fixed location. Once concentrated $CO_2$ is captured, geological formations and aquifers, depleted oil and natural gas reservoirs, and deep coal beds are possible locations to sequester the carbon dioxide (See Figure 1.3). If the goal is $CO_2$ storage rather than oil recovery, then depleted or nearly depleted oil fields may be used for sequestration even if they are not good candidates for enhanced oil recovery. The porous and permeable rock layer that contains fluids is covered by an impermeable cap rock. Normally, oil and natural gas will tend to migrate upward through permeable rock but the cap rock traps them. Since oil and natural gas have been sequestered in such formations for millions of years, there is good reason to believe that $CO_2$ will remain there as well. The cross section of a typical oil reservoir is depicted in Figure 1.4. Deep seated aquifers and coal beds are another suitable location for sequestration of $CO_2$. One project is currently on at Sleipner field in the North Sea (see Figure 1.5) off the coast of Norway.

However, the issues involved in geological sequestration are more complicated than those of EOR. Firstly, for sequestration to be effective, the $CO_2$ needs to be stored for hundreds of years and it is difficult to predict at this point if it will be effective. Secondly, there is the possibility of $CO_2$ escaping through abandoned wells of an oil field. Another

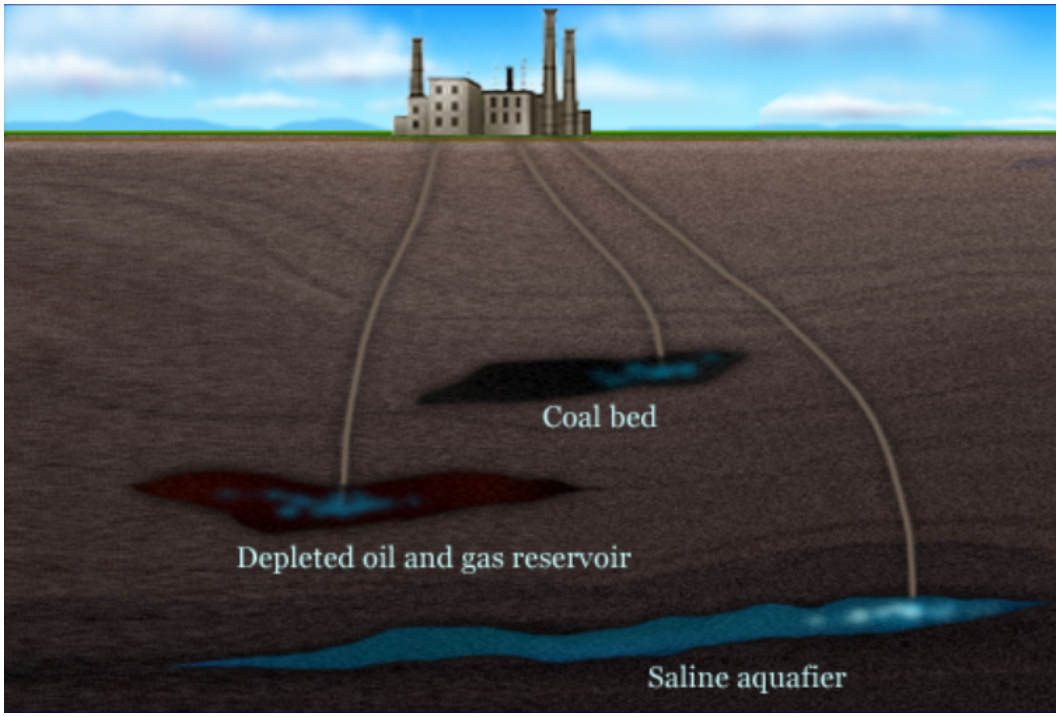


Figure 1.3: Carbon sequestration process (Source: `http://www.planetseed.com/node/15250`)

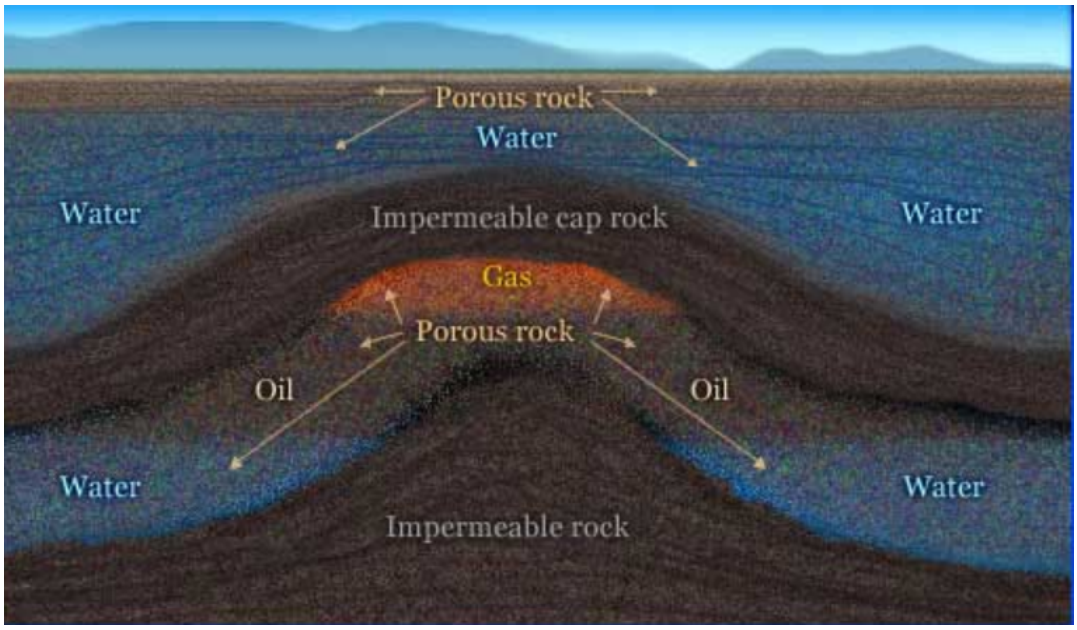


Figure 1.4: Cross section of a typical oil reservoir (Source: `http://www.planetseed.com/node/15250`)

possible pathway for $CO_2$ to leak would be cracks in the cap rock. $CO_2$ sequestration is proposed for regions that are geologically stable, where earthquakes are not likely to occur. However, the sequestering of $CO_2$ itself could result in increased pressure under the cap rock that could result in cracks. The solution is to monitor pressure and take care not to exceed the limits of the formation. The reader may consult [3] for details on the challenges posed by this problem.

While $CO_2$ is not poisonous, it can cause death by suffocation if there is uncontrolled release. One such catastrophe occurred at Lake Nyos where on August 21, 1986, there was a sudden release of $CO_2$, which flowed into valleys around the lake and killed 1,700 people in nearby villages (see Figure 1.6).

Analogous to the EOR process where the yield at the production well is of importance, here safety concerns dictate that it is paramount to predict the rate of leakage of $CO_2$. Thus the main thrust of modelling in both these processes (EOR and CS) is accurate prediction of fluid flux or leakage [4, 5, 6, 7].

However, neglecting for now the differences between EOR and carbon sequestration, the complexities of the physical processes in EOR enumerated earlier apply equally to carbon sequestration.

## 1.2 Modelling efforts

In principle, one could write down the balance laws for fluid motion through the porous medium knowing the spatial distribution of the pores and solve for the velocity field after enforcing appropriate boundary conditions at the fluid-pore interface. This is a hopeless task, however, for even if the spatial distribution were known, the problem is intractable. Hence one has to abandon the microscopic view and move to a macroscopic viewpoint, where one can deal with certain "average" quantities that represent the macroscopic behaviour.

The methods of volume averaging and homogenization have been used to this effect [8, 9, 10]. We shall not discuss them further, for our focus is on the third technique, that of mixture theory or the theory of interacting continua. The theory is particularly well

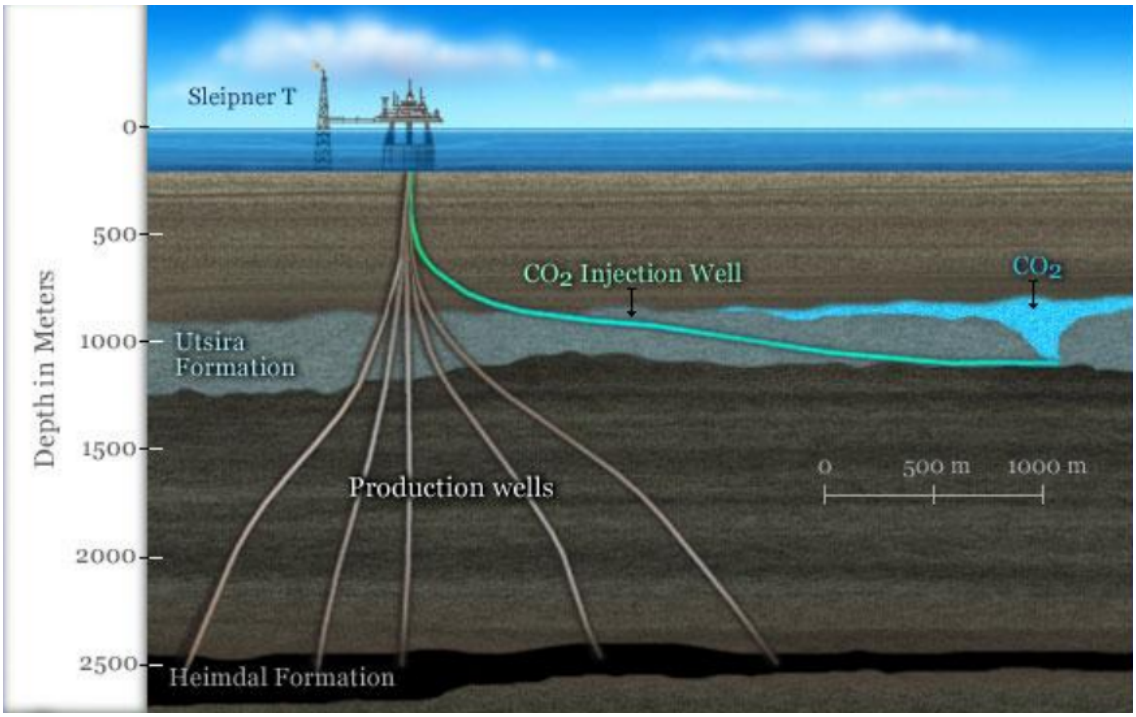


Figure 1.5: Carbon sequestration at Sleipner (Source: `http://www.planetseed.com/node/15252`)

Figure 1.6: Hazards of carbon sequestration: In 1986, Lake Nyos released a large cloud of $CO_2$ , which suffocated 1700 people and 3500 livestock in nearby villages (Source: `http://www.waterencyclopedia.com/Hy-La/Lakes-Chemical-Processes.html`)

suited to the study of flow of fluids through porous media. We shall discuss the general framework of mixture theory in the next section, so for now we remark merely that the theory allows for relative motion between the constituents of the mixture, ensures that each component of the mixture meets all the balance laws and also takes into account the various interactions that are possible within the constituents of the mixture including chemical reactions and inter-conversion between the constituents.

### *1.2.1 Popular models*

We record the equations that represent some of the popular models for flow of fluids through porous media.

Let grad[·] denote the Eulerian gradient while div[·] denotes the Eulerian divergence operator.

We denote the velocity field by $\boldsymbol{v}(\boldsymbol{x})$, the pressure by $p$, and define the "drag coefficient" $\alpha$ related to the permeability of the medium $k$ and the viscosity of the fluid $\mu$ by

$$\alpha = \frac{\mu}{k} \tag{1.1}$$

The classical Darcy equations [11] are given by the system

$$\text{grad}[p] + \alpha \boldsymbol{v} = \rho \boldsymbol{b}, \tag{1.2a}$$

$$\text{div}[\boldsymbol{v}] = 0 \tag{1.2b}$$

where $\rho$ is the density of the fluid, and $\boldsymbol{b}(\boldsymbol{x})$ is the specific body force. It has been applied to study problems in groundwater hydrology [12, 13], EOR [14, 15] and CS [5, 16].

The Forchheimer equations [17] are a modification of the classical Darcy model, where the "drag coefficient" is no longer a constant, instead

$$\text{grad}[p] + \alpha(\|\boldsymbol{v}\|)\boldsymbol{v} = \rho \boldsymbol{b}, \tag{1.3a}$$

$$\text{div}[\boldsymbol{v}] = 0 \tag{1.3b}$$

The classical Brinkman equation [18, 19] is given by the system

$$\alpha \boldsymbol{v} + \text{grad}[p] - 2\mu\Delta\boldsymbol{v} = \rho\boldsymbol{b} \tag{1.4a}$$

$$\text{div}[\boldsymbol{v}] = 0 \tag{1.4b}$$

where, $\Delta(\cdot) := \text{div}[\text{grad}(\cdot)]$ is the Laplacian operator, all other quantities having been previously defined. Although it has not enjoyed the same popularity as the Darcy model, applications of the Brinkman equation in porous media do occur, as in [20, 21, 22].

### 1.3 Variation of material properties under extreme conditions

It was mentioned earlier that under high pressures and elevated temperatures, the material properties of the fluid like viscosity and density could change. There exists irrefutable experimental evidence that the viscosity of a fluid depends on the pressure. The history of the early experimental results concerning the same can be found in the book by Bridgman [23] on the physics of high pressure. Stokes [24] was aware of the viscosity of the fluid depending on the pressure and as early as 1893 Barus [25] suggested an exponential dependence of the viscosity on the pressure based on his experimental investigations. There has been a great deal of experimental data since Bridgman's book that document the variation of viscosity with pressure (see [26, 27, 28, 29, 30, 31, 32, 33, 34, 35, 36, 37]). In most liquids, while the variation in the viscosity can be of the order of $10^8$ (see Bair and Kottke [36]), the variation of the density due to variation in the pressure is of the order of a few percent (see Dowson and Higginson [38], Rajagopal [39]), and thus it would be reasonable to assume that the liquid is still incompressible while the visocity varies with the pressure.

Barus [25] suggested an exponential dependence of the viscosity on the pressure, i.e.,

$$\mu(p) = \mu_0 \exp(\beta p), \quad \mu_0 > 0,\ \beta \geq 0, \tag{1.5}$$

where $\mu_0$ and $\beta$ are constants , with $\mu_0$ having the dimension of viscosity and $\beta$ the

dimension that is the inverse of that of the pressure.

Bridgman [23] in his book cites a personal communication from Andrade that provides a relationship of the viscosity to the temperature, density and pressure [1] (see also the discussion in [41]).

$$\mu(p, \rho, \theta) = A\rho^{\frac{1}{2}} \exp\left((p + \rho^2 r)\frac{s}{\theta}\right), \tag{1.6}$$

where $\theta$ denotes the temperature, $A, r$ and $s$ are constants, and $\rho$ denotes the density.

Pressure-viscosity data and approximate values of the pressure-viscosity coefficient $\beta$ in Barus formula for mineral and vegetable oils are reported in [42, 43, 44]. For supercritical carbon-dioxide, in the range 0.1 MPa to 8000 MPa the variation of viscosity with pressure at various temperatures is reported in [45, 46]. These experimental studies clearly indicate that the viscosity varies exponentially with respect to pressure even for supercritical carbon-dioxide for various temperatures and for a wide range of pressures. Hence we conclude that viscosity cannot be assumed constant in the operating pressure range of EOR and carbon sequestration.

From equation (1.5) and (1.6), it is clear that the viscosity increases with increasing pressure but decreases with increasing temperature. These are competing effects and depending on the process, one effect may dominate the other.

## 1.4 Limitations of the popular models

Rajagopal [47] has shown that, within the context of theory of mixtures, the Darcy equation can be obtained after making a plethora of assumptions about the solid and the fluid. The restrictions under which the Darcy equation was derived are rather stringent, and in [47], the assumptions are systematically relaxed and an hierarchy of models is thus obtained, where the Darcy model is the one derived under the most restrictive assumptions. The reader is directed to references [48, 49, 50] for a detailed derivation of Darcy's equation using the theory of mixtures.

Far from being a "law" with universal classical Darcy's equation, which is an approxi-

[1] Attempts to locate the paper by Andrade wherein that formula is given have been unsuccessful thus far. The reference to Andrade [40] that Bridgman provides does not contain the formula mentioned.

mation to the balance of linear momentum is reasonable only if

1. The solid is a saturated rigid porous body whose balance of linear momentum can be ignored. The stresses developed in the rigid solid body being that which is necessary to meet the balance of linear momentum.

2. The pore structure in the solid is uniform and hence there is no inhomogeneity in the pore structure.

3. The flow is sufficiently slow so that the inertial effects in the fluid can be neglected.

4. The frictional effects in the fluid due to the viscosity of the fluid can be neglected.

5. The only interaction between the solid and the fluid is due to the friction at the pores and is proportional to the relative velocity between the solid and the fluid.

6. The flow is steady.

7. The fluid is incompressible.

8. The pressure range that the fluid is subject to does not lead to changes in the viscosity of the fluid.

9. The partial stress in the fluid is that in an Euler fluid.

The Forchheimer model is obtained if one modifies item (5) above to allow the drag coefficient to depend on the magnitude of the relative velocity between the solid and the fluid. The classical Brinkman model is obtained by relaxing the assumptions (4) and (9) given above and assuming the partial stress in the fluid to be given by the classical incompressible Navier-Stokes constitutive equation and taking into account the viscous effects in the fluid.

It is easy to see that the assumptions are very restrictive; a real physical problem violates one or more of these assumptions frequently. The models named thus far are incapable of predicting the stresses in a deforming porous media, the inertial effects of the flow, or

take into account other interaction forces between the solid and the fluid. The problems of EOR and CS have several features that make them complicated as discussed earlier, and some of them violate the assumptions under which the models of Darcy, Forchheimer and Brinkman are derived. The change in material properties under high pressure gradients is specially important in EOR and CS, and we estimate the magnitude of this effect with a simple example.

The change in density under the operating pressures, say $p_0$ =1 atm, $p_1 = 600\,\text{atm}$ is calculated from the Dowson-Higginson formula $\rho(p) = \rho_0 \left[1 + \frac{0.6p}{1+1.7p}\right]$, $p$ in GPa, and the relative percent change in density is less than 3.5 % but using Barus formula $\mu(p) = \mu_0 \exp[\beta p]$ with $\beta^{-1} = 40\,\text{MPa}$, i.e., $\beta = 2.5 \times 10^{-3}\,\text{atm}^{-1}$ the relative percent change in viscosity is almost 350 %. Thus density changes may be neglected and the assumption of incompressibility is realistic, but the change in viscosity is clearly too large to be neglected.

One cannot expect at the outset to develop a model that can incorporate all the complexities that characterize the problem of EOR and CS, considering the fact that some of the features such as the fracturing of the solid remain daunting open problems even when no fluid flow is involved. Considering that Darcy's equation is still the most popular model for describing flow through porous media, it would be prudent to incorporate the various complexities in a gradual manner and solve the problem as a sequence of problems.

With this in mind, in this dissertation we shall proceed in steps:

(a) In Section 2 we shall derive generalizations of the popular models that take into account the viscous effects in the fluid and also the fact that the viscosity and the drag depend upon the pressure. We shall however ignore the deformation of the solid and consider it to be rigid. The approach differs from conventional mixture theory in that we will be using the hypothesis of maximization of the rate of entropy production to derive the results.

(b) Using a generalized Brinkman model obtained previously in Section 2, we shall study the problem of steady flow in a slab under large pressure gradients in Section 3.

(c) Then we shall relax assumption (2) and allow the permeability of the porous medium to be non-uniform and anisotropic, i.e., the permeability to the flow may not be the same in all directions.

(d) Subsequently in Section 5, while still neglecting the deformation of the solid, we shall consider unsteady flow engendered by a pulsatile forcing pressure and compare the response to a constant forcing pressure.

The case of a deforming porous media has not been dealt with in this work, but the results obtained here for a rigid porous medium clearly indicate that the flow rate, which is the main quantity of interest, differs qualitatively and quantitatively from that predicted by classical models, and it makes a compelling case for the use of models that incorporate the pressure dependence of viscosity.

# 2. A THERMODYNAMIC BASIS FOR THE DERIVATION OF THE DARCY-FORCHHEIMER-BRINKMAN MODELS FOR FLOWS THROUGH POROUS MEDIA AND THEIR GENERALIZATIONS

Mixture theory provides a thermodynamic framework to study the interactions between a complex agglomeration, including the production and destruction of the constituents, of the mixture due to external stimuli. The origins of mixture theory can be traced back to the seminal contributions due to Fick [51] and Darcy [11]. The mathematical foundations of mixture theory were laid down by Truesdell [52], [53]. The basic premise of the theory is that at each point in space occupied by the mixture, there is a particle belonging to every constituent of the mixture, that is, in a homogenized sense there is co-occupancy by the constituents of the mixture. Of course, co-occupancy is a physical impossibility. It is assumed that each of the constituents is dense enough in the mixture to be homogenized over the region occupied by the mixture and treated as a continuum in its own right. Just as for a single constituent continuum, one can define motion, mass density, partial stress tensor, temperature, internal energy, entropy and other relevant physical quantities for each constituent of the mixture as it moves relative to the other constituents due to the applied forces.

It is customary to postulate the balance laws for mass, linear momentum, angular momentum and energy for individual constituents of the mixture and assume suitable constitutive equations for the quantities like stress, specific energy, heat flux, etc. of each constituent as well as the various interactions between the different constituents. Thereafter, one appeals to the second law of thermodynamics to obtain restrictions for the allowable forms for the constitutive equations. The reader is directed to [54], [55], [49], [48], [50] and the books by Samohyl [56] and Rajagopal and Tao [57] for the details.

The theory of mixtures lends itself to a convenient description of the flow of fluids through porous solids. Darcy's model [11], which is widely used even today, is one of the

early attempts at describing the flow of a single fluid through a rigid porous solid, due to a pressure gradient. It can be shown that Darcy's model can be obtained from the framework of mixture theory by making a host of assumptions about the solid and the fluid (See Munaf *et al.* [13]). The assumptions include neglecting the deformation of the solid and assuming it to be rigid, assuming the flow to be steady, neglecting viscous effects within the fluid, assuming a special form for the drag due to the friction at the pores, and several others. While the classical Darcy model provides good agreement in many physical situations, large departures from the predictions of the model are also prevalent as in [58], [59]. Various generalizations of Darcy's model, like the Forcheimmer equation [17], have been proposed to remedy this shortcoming. The restrictions under which the Darcy model was derived are rather stringent, and in [47], the assumptions are systematically relaxed and an hierarchy of models is obtained, the Darcy model being the one derived under the most restrictive assumptions. The Brinkman model [18], [19] is another popular model, obtained when viscous effects within the fluid are not neglected and instead are modelled as those of the classical incompressible Navier-Stokes fluid. However, like in the case of the Darcy model, various generalizations have been made, and in [47], one can find a record of these various generalizations of the classical Darcy and Brinkman models. In this article, we derive the familiar Darcy and Brinkman models that are used to describe the flow of fluids through porous media, and their generalizations, by appealing to the requirement that the rate of entropy production be maximized. This is a more stringent requirement than the second law of thermodynamics which requires that the rate of entropy production be non-negative. Such an approach has been used successfully in a number of studies to obtain a variety of material responses (see [60], [61], ,[62],[63], [64]) but within the context of the theory of mixtures, the only relevant study is that provided by [65] which deals with a mixture of two fluids. The present article is different in that we do not consider a mixture of two fluids; rather we consider a mixture of a solid and a fluid and assume that the solid behaves like a rigid body.

The organization of the section is as follows: In Section 2.1 we outline the conventions

and notations and summarize the governing equations for a mixture of a solid and a fluid. In Section 2.3, we discuss the constitutive assumptions for the components of the mixture. We illustrate the use of the criterion of maximization of rate of entropy production in Section 2.4 following which we obtain the Brinkman model and its generalizations in Section 2.5 while Section 2.6 is devoted to a similar effort for obtaining the Darcy model. Section 2.7 is devoted to some concluding remarks.

## 2.1 Preliminaries

First we record the balance equations for a mixture of two constituents, a solid and a fluid. The quantities associated with the fluid are indicated by the superscript $f$ while those associated with the solid are indicated by the superscript $s$. The superscript $i$ signifies that we are referring to the $i^{\text{th}}$ constituent.

Let grad$[\cdot]$ denote the Eulerian gradient and div$[\cdot]$ the Eulerian divergence operator. We represent the identity tensor by $\boldsymbol{I}$ and the inner product of any two tensors $\boldsymbol{A}, \boldsymbol{B}$ is defined through $\boldsymbol{A} \cdot \boldsymbol{B} := \text{tr}[\boldsymbol{A}^T \boldsymbol{B}]$, where $(\cdot)^T$ denotes the transpose of a linear transformation. The symbol $\|\cdot\|$ will be used to denote the norm of a vector or a tensor, where the norm of a tensor is defined by $\|\cdot\| := \sqrt{\text{tr}[(\cdot)^T(\cdot)]}$.

We denote by $\boldsymbol{v}^i$ the velocity field of the $i^{\text{th}}$ constituent and the material time derivative with respect to the $i^{\text{th}}$ constituent is given by

$$\frac{d^{(i)}(\cdot)}{dt} := \frac{\partial(\cdot)}{\partial t} + \text{grad}[\cdot] \cdot \boldsymbol{v}^i \tag{2.1}$$

We also define the following kinematical quantities

$$\boldsymbol{L}^i := \text{grad}[\boldsymbol{v}^i], \tag{2.2}$$

$$\boldsymbol{D}^i := \frac{1}{2}[\boldsymbol{L}^i + (\boldsymbol{L}^i)^T] \tag{2.3}$$

which are pertinent to our calculations.

## 2.2 Summary of governing equations

The balance of mass for each of the constituents in the absence of interconversion of mass due to chemical reactions takes the form

$$\frac{d^{(i)}\rho^i}{dt} + \rho^i \mathrm{div}[\boldsymbol{v}^i] = 0,\ i = s, f \tag{2.4}$$

where $\rho^i$ is the density of the $i^{\text{th}}$ constituent.

Let $\boldsymbol{t}^i$ denote the partial traction associated with the $i^{\text{th}}$ constituent. Then if $\boldsymbol{T}^i$ denotes the partial stress of the $i^{\text{th}}$ constituent,

$$\boldsymbol{t}^i = (\boldsymbol{T}^i)^T \boldsymbol{n},\ i = s, f \tag{2.5}$$

where $\boldsymbol{n}$ is the outward unit normal.

The balance of linear momentum for each of the constituents is given by

$$\mathrm{div}[\boldsymbol{T}^i]^T + \rho^i \boldsymbol{b}^i + \boldsymbol{m}^i = \rho^i \frac{d^{(i)}\boldsymbol{v}^i}{dt},\ i = s, f \tag{2.6}$$

where $\boldsymbol{T}^i$ is the (partial) Cauchy stress, $\boldsymbol{m}^i$ is the interaction force acting on the $i^{\text{th}}$ constituent due to the other constituents and $\boldsymbol{b}^i$ is the specific body force.

Since there can be no net production of momentum, summing over $i = s, f$ yields

$$\boldsymbol{m}^s + \boldsymbol{m}^f = \boldsymbol{0} \tag{2.7}$$

The balance of angular momentum in the absence of body couples and angular momentum supply reduces to

$$\boldsymbol{T}^i = (\boldsymbol{T}^i)^T,\ i = s, f. \tag{2.8}$$

The balance of energy is given by

$$\rho^i \frac{d^{(i)}}{dt}\left(\epsilon^i + \frac{1}{2}\boldsymbol{v}^i \cdot \boldsymbol{v}^i\right) = \mathrm{div}[\boldsymbol{T}^i \boldsymbol{v}^i - \boldsymbol{q}^i] + \boldsymbol{m}^i \cdot \boldsymbol{v}^i + \rho^i \boldsymbol{b}^i \cdot \boldsymbol{v}^i + \rho^i r^i + E^i,\ i = s, f \tag{2.9}$$

where $\epsilon^i$ is the specific internal energy, $\boldsymbol{q}^i$ the specific heat flux , $r^i$ the specific radiant heating and $E^i$ is the energy supply to the $i^{\text{th}}$ constituent.

Since there is no net production of energy, summing over $i = s, f$ yields

$$(E^f + E^s) + (\boldsymbol{m}^s \cdot \boldsymbol{v}^s + \boldsymbol{m}^f \cdot \boldsymbol{v}^f) = 0 \tag{2.10}$$

Using equation (2.6) and equation (2.4), we can simplify equation (2.9) to

$$\rho^f \frac{d^{(f)}\epsilon^f}{dt} = \boldsymbol{T}^f \cdot \boldsymbol{L}^f - \operatorname{div}[\boldsymbol{q}^f] + \rho^f r^f + E^f = 0, \tag{2.11a}$$

$$\rho^s \frac{d^{(s)}\epsilon^s}{dt} = \boldsymbol{T}^s \cdot \boldsymbol{L}^s - \operatorname{div}[\boldsymbol{q}^s] + \rho^s r^s + E^s = 0 \tag{2.11b}$$

We adopt the local form of the Clausius-Duhem inequality for the mixture as a whole as the statement of the second law.[1] We also assume that at a given time instant and position, all the constituents have a common temperature $\theta$. Thus, we obtain:

$$\rho^f \frac{d^{(f)}\eta^f}{dt} + \rho^s \frac{d^{(s)}\eta^s}{dt} + \operatorname{div}\left[\frac{\boldsymbol{q}^s + \boldsymbol{q}^f}{\theta}\right] - \left[\frac{\rho^s r^s + \rho^f r^f}{\theta}\right] = \eta_{\text{prod}} \geq 0 \tag{2.12}$$

where $\eta_{\text{prod}}$ is the production of entropy from the mixture as a whole and is non-negative as per the statement of the second law of thermodynamics.

We now introduce the specific Helmholtz potential $\psi^i$ for the constituents through

$$\psi^i = \epsilon^i - \theta\eta^i. \tag{2.13}$$

It follows from the Clausius-Duhem inequality that

$$\frac{\partial \psi^i}{\partial \theta} = -\eta^i, \tag{2.14}$$

[1] Even within the context of a single continuum, there are fundamental issues concerning the use of the local form of the second law of thermodynamics and the usual procedure of requiring that the body be subject to arbitrary thermodynamic processes (See [62] for a more detailed discussion).

Using equation (2.13) and equation (2.14) in equation (2.12), equation (2.11) along with equation (2.10) and equation (2.7) yields

$$\xi := \theta\eta_{\text{prod}} = \boldsymbol{T}^f \cdot \boldsymbol{L}^f + \boldsymbol{T}^s \cdot \boldsymbol{L}^s + \boldsymbol{m}^s \cdot \boldsymbol{v}_{\text{rel}} - \rho^f \left.\frac{d^{(f)}\psi^f}{dt}\right|_\theta - \rho^s \left.\frac{d^{(s)}\psi^s}{dt}\right|_\theta - \frac{\text{grad}[\theta] \cdot (\boldsymbol{q}^f + \boldsymbol{q}^s)}{\theta} \geq 0 \tag{2.15}$$

where $\boldsymbol{v}_{\text{rel}} := \boldsymbol{v}^f - \boldsymbol{v}^s$ is the relative velocity of the fluid with respect to the solid.

The equation equation (2.15) is a general form of the reduced dissipation equation in terms of the Helmholtz potential for a mixture of a solid and a fluid with no mass exchange between them. We shall simplify this equation for particular cases in the next section.

## 2.3 Constitutive assumptions

We now make the constitutive assumptions pertinent to the constituents of the mixture and simplify the governing equations which have been obtained thus far.

1. We assume that the solid is an idealized rigid solid. Hence the strain $\boldsymbol{\varepsilon}^s \equiv \boldsymbol{0}$, along with $\boldsymbol{D}^s \equiv \boldsymbol{0}$ for all motions of the solid.

2. We shall neglect thermal effects and consider only isothermal processes that take place at a constant temperature $\theta^*$.

3. We shall assume that the fluid is incompressible, i.e., it can only undergo isochoric motions. The constraint of incompressibility for the fluid can then be expressed in any of the following equivalent ways as follows:

$$\text{div}[\boldsymbol{v}^f] = \text{tr}\boldsymbol{L}^f = \text{tr}\boldsymbol{D}^f = \boldsymbol{D}^f \cdot \boldsymbol{I} = \boldsymbol{L}^f \cdot \boldsymbol{I} = 0. \tag{2.16}$$

4. We neglect transient and inertial effects so that $\dfrac{d^{(i)}\boldsymbol{v}^i}{dt} \approx \boldsymbol{0},\ i = s, f$. This assumption will be used later on.

The partial stress of the fluid is decomposed as

$$\boldsymbol{T}^f = -p^f \boldsymbol{I} + \hat{\boldsymbol{T}}^f \tag{2.17}$$

where $p^f := -\dfrac{\mathrm{tr}\boldsymbol{T}^f}{3}$ is the mean normal stress and $\hat{\boldsymbol{T}}^f$ is the deviatoric part of the stress. Such a decomposition is unique and using it in light of the assumptions $(1)-(3)$ in equation (2.15), yields

$$\xi := \theta\eta_{\mathrm{prod}} = \left[\hat{\boldsymbol{T}}^f \cdot \boldsymbol{D}^f + \boldsymbol{m}^s \cdot \boldsymbol{v}_{\mathrm{rel}} - \rho^f \frac{d^{(f)}\psi^f}{dt}\bigg|_{\theta^*} - \rho^s \frac{d^{(s)}\psi^s}{dt}\bigg|_{\theta^*}\right] \geq 0 \tag{2.18}$$

We assume that the state variables are

$$\mathcal{S} = \left\{\boldsymbol{D}^f, \boldsymbol{v}_{\mathrm{rel}}\right\} \tag{2.19}$$

The set of state variables has been chosen on the basis of the assumptions made above. If the fluid were not incompressible for instance, then $\mathrm{tr}\boldsymbol{D}^f$ would also be considered a state variable.

## 2.4 Maximization of the rate of entropy production

At this juncture it is appropriate to make a remark on the usage of the Helmholtz and Gibbs potential in the context of modelling a rigid solid. The Helmholtz potential usually depends on the temperature, appropriate kinematical variables (usually the deformation gradient and its higher time or spatial derivatives) , amongst other appropriate variables, and the Gibbs potential on the other hand depends on the temperature, stress and other appropriate variables. However, the stress in a rigid body is indeterminate, or put differently it can be whatever it needs to be so that the boundary conditions are met. It thus makes no sense to define the Gibbs potential for such a body as the Gibbs potential is based on the stress.

On the other hand, the strain in a rigid body is zero (or to be more precise, the deformation gradient in a rigid body corresponding to a rigid motion is an orthogonal

tensor, since a rigid body is one wherein the distance between any two points pairwise remains the same for all time), and the Helmholtz potential for the body could depend on the temperature, and possibly other variables. It is usually assumed that the Helmholtz potential is a function of temperature [66] and this leads to the familiar equation governing heat conduction in a rigid solid. The assumption is not strictly in accordance with the definition of a rigid body, but it all depends on what one means by temperature.

If by temperature one means the random thermal agitation of the molecules, then one has the problem of what one means by a rigid body as this thermal agitation would mean that the distance between the randomly agitating points (particles) constituting the body would change. We cannot get into these sorts of issues here. In a recent paper Rajagopal [67] outlines the difficulties that are inherent with the notion of "points" in mathematics and particles in mechanics and hence the difficulty with regard to even defining what is meant by distance between "points".

Ideally, we ought to assume that in a rigid body, the Helmholtz potential is a constant. However, since the temperature is assumed to be constant in the problem that we are considering (in fact we are assuming that the processes are isothermal in deriving the equations due to Darcy, Forchheimer and Brinkman), the Helmholtz potential for the mixture is essentially the Helmholtz potential of the fluid. If the solid were deformable, then we could define an appropriate Helmholtz potential for the deforming solid.

We shall now pick specific forms for the Helmholtz potential of the fluid $\psi^f(\boldsymbol{D}^f, \boldsymbol{v}_{\rm rel}, \theta^*)$ and the rate of dissipation $\xi(\boldsymbol{D}^f, \boldsymbol{v}_{\rm rel}, \theta^*)$ of the mixture such that $\xi$ is nonnegative. The arguments are frame indifferent quantities and hence the functions so defined are automatically frame indifferent scalars.

Maximizing $\xi$ subject to the constraint given by equation (2.18) and equation (2.16) yields constitutive equations for the material. We assume that the Helmholtz potential

$$\psi^f = \psi^f(\theta^*), \tag{2.20}$$

which immediately implies that in this case

$$\left.\frac{d^{(f)}\psi^f}{dt}\right|_{\theta^*} = 0 \tag{2.21}$$

$$\left.\frac{d^{(s)}\psi^s}{dt}\right|_{\theta^*} = 0 \tag{2.22}$$

Thus equation (2.15) further simplifies to

$$\xi = \hat{\boldsymbol{T}} \cdot \boldsymbol{D} + \boldsymbol{m} \cdot \boldsymbol{v}_{\text{rel}} \geq 0 \tag{2.23}$$

where the superscripts have now been dropped for convenience.

We maximize $\xi$ with respect to $\boldsymbol{D}$ and $\boldsymbol{v}_{\text{rel}}$ over all $\boldsymbol{D}$ that are traceless, i.e., $\boldsymbol{D} \cdot \boldsymbol{I} = 0$ and the constraint equation (2.23) We utilize the method of Lagrange multipliers, and construct the auxiliary function that we wish to maximize:

$$\Phi(\boldsymbol{D}, \boldsymbol{v}_{\text{rel}}) := \xi + \lambda_1(\xi - \hat{\boldsymbol{T}} \cdot \boldsymbol{D} - \boldsymbol{m} \cdot \boldsymbol{v}_{\text{rel}}) + \lambda_2(\boldsymbol{D} \cdot \boldsymbol{I}). \tag{2.24}$$

The necessary condition for an extremum then yields

$$\frac{\partial \Phi}{\partial \boldsymbol{D}} = 0 \;\Rightarrow\; \phi_1 \frac{\partial \xi}{\partial \boldsymbol{D}} - \hat{\boldsymbol{T}} + \phi_2 \boldsymbol{I} = \boldsymbol{0}, \tag{2.25a}$$

$$\frac{\partial \Phi}{\partial \boldsymbol{v}_{\text{rel}}} = 0 \;\Rightarrow\; \phi_1 \frac{\partial \xi}{\partial \boldsymbol{v}_{\text{rel}}} - \boldsymbol{m} = \boldsymbol{0}, \tag{2.25b}$$

where $\phi_1 := \dfrac{1+\lambda_1}{\lambda_1},\ \phi_2 := \dfrac{\lambda_2}{\lambda_1}$.

Multiplying equation (2.25a), equation (2.25b) by $\boldsymbol{D},\ \boldsymbol{v}_{\text{rel}}$ respectively and adding, we obtain

$$\phi_1 \left[ \frac{\partial \xi}{\partial \hat{\boldsymbol{T}}} \cdot \hat{\boldsymbol{T}} + \frac{\partial \xi}{\partial \boldsymbol{v}_{\text{rel}}} \cdot \boldsymbol{v}_{\text{rel}} \right] - \xi = 0, \tag{2.26}$$

while taking inner product of equation (2.25a) with $\boldsymbol{I}$ yields

$$\phi_2 = -\frac{\phi_1}{3} \left[ \frac{\partial \xi}{\partial \boldsymbol{D}} \cdot \boldsymbol{I} \right] = -\frac{\phi_1}{3} \text{tr} \left[ \frac{\partial \xi}{\partial \boldsymbol{D}} \right]. \tag{2.27}$$

We have used the fact that $\boldsymbol{D}\cdot\boldsymbol{I}=0,\ \boldsymbol{I}\cdot\boldsymbol{I}=3$.

We introduce the notation $[\cdot]_{\text{dev}}$ to denote the deviatoric part of a tensor and by using equation (2.26) and equation (2.27) in equation (2.25)

$$\hat{\boldsymbol{T}}=\phi_1\left[\frac{\partial\xi}{\partial\boldsymbol{D}}\right]_{\text{dev}}, \tag{2.28a}$$

$$\boldsymbol{m}=\phi_1\frac{\partial\xi}{\partial\boldsymbol{v}_{\text{rel}}}, \tag{2.28b}$$

$$\text{and}\ \ \phi_1=\xi\left[\frac{\partial\xi}{\partial\boldsymbol{D}}\cdot\boldsymbol{D}+\frac{\partial\xi}{\partial\boldsymbol{v}_{\text{rel}}}\cdot\boldsymbol{v}_{\text{rel}}\right]^{-1}. \tag{2.28c}$$

By making specific choices for the rate of dissipation $\xi$, we can obtain different types of models. Of course, the choice of $\xi$ is dictated by the physics of the problem.

## 2.5 Generalizations of Brinkman's model

Consider

$$\xi(\boldsymbol{D},\boldsymbol{v}_{\text{rel}})=\alpha(p,\hat{\boldsymbol{T}},\boldsymbol{m})\|\boldsymbol{v}_{\text{rel}}\|^2+2\mu(p,\hat{\boldsymbol{T}},\boldsymbol{m})\|\boldsymbol{D}\|^2,\ \ \text{where}\ \alpha>0,\ \mu>0. \tag{2.29}$$

It is clearly non-negative and moreover, $\xi(\boldsymbol{0},\boldsymbol{0})=0$. The functional form chosen suggests that the total dissipation comes from two sources; the dissipation at the pores of the solid due to the flow of the fluid and the dissipation due to viscous effects within the fluid bulk.

On using the form equation (2.29) and on substituting it into equation (2.28), we obtain

$$\hat{\boldsymbol{T}}=2\mu(p,\hat{\boldsymbol{T}},\boldsymbol{m})\boldsymbol{D}, \tag{2.30a}$$

$$\boldsymbol{m}=\alpha(p,\hat{\boldsymbol{T}},\boldsymbol{m})\boldsymbol{v}_{\text{rel}}. \tag{2.30b}$$

As they stand, the formulae equation (2.30a) and equation (2.30b) are yet general as specific choices have not been made for the viscosity $\mu$ and the drag coefficient $\alpha$. In contrast to the conventional approach, the constitutive equations obtained are for the kinematical quantities $\boldsymbol{D},\boldsymbol{v}_{\text{rel}}$ as a function of $p,\hat{\boldsymbol{T}},\boldsymbol{m}$. We shall now consider various specific choices for $\mu$ and $\alpha$. We shall also fix the frame to the solid so that $\boldsymbol{v}^s\equiv\boldsymbol{0},\quad \boldsymbol{v}_{\text{rel}}\equiv\boldsymbol{v}^f,\quad \boldsymbol{D}_{\text{rel}}\equiv\boldsymbol{D}^f$

and drop the superscript $f$ for convenience.

Some particular choices are:

1. $\alpha(p, \hat{\boldsymbol{T}}, \boldsymbol{m}) = \alpha_0,\ \mu(p, \hat{\boldsymbol{T}}, \boldsymbol{m}) = \mu_0$, where $\alpha_0,\ \mu_0$ are positive constants, leads to the standard Brinkman model $\boldsymbol{T} = -p\boldsymbol{I} + 2\mu_0\boldsymbol{D},\ \boldsymbol{m} = \alpha_0\boldsymbol{v}_{\text{rel}}$, which in turn leads to the following governing equation[2]

$$\alpha_0\boldsymbol{v} + \text{grad}[p] - \text{div}[2\mu_0\boldsymbol{D}] = \rho\boldsymbol{b}, \tag{2.31a}$$

$$\text{div}[\boldsymbol{v}] = 0. \tag{2.31b}$$

2. $\alpha(p, \hat{\boldsymbol{T}}, \boldsymbol{m}) = \alpha(p) > 0,\ \mu(p, \hat{\boldsymbol{T}}, \boldsymbol{m}) = \mu(p) > 0$ leads to a generalization of the Brinkman model where both the viscosity and drag coefficient depend on the pressure (or the mean normal stress) $\boldsymbol{T} = -p\boldsymbol{I} + 2\mu(p)\boldsymbol{D},\ \boldsymbol{m} = \alpha(p)\boldsymbol{v}_{\text{rel}}$. In this case, the governing equation reduces to:

$$\alpha(p)\boldsymbol{v} + \text{grad}[p] - \text{div}[2\mu(p)\boldsymbol{D}] = \rho\boldsymbol{b}, \tag{2.32a}$$

$$\text{div}[\boldsymbol{v}] = 0. \tag{2.32b}$$

3. The choice $\alpha(p, \hat{\boldsymbol{T}}, \boldsymbol{m}) = \alpha_0 + \alpha_1\|\boldsymbol{m}\|$, where $\alpha_0,\ \alpha_1$ are positive constants, leads to

$$\boldsymbol{m} = [\alpha_0 + \alpha_1\|\boldsymbol{m}\|]\boldsymbol{v}_{\text{rel}}. \tag{2.33}$$

This implies $\|\boldsymbol{m}\| = \dfrac{\alpha_0\|\boldsymbol{v}_{\text{rel}}\|}{1 - \alpha_1\|\boldsymbol{v}_{\text{rel}}\|}$ and clearly, $\alpha_1\|\boldsymbol{v}_{\text{rel}}\| < 1$

Substituting $\|\boldsymbol{m}\|$ in equation (2.33) and approximating

$$(1 - z)^{-1} \approx 1 + z \text{ when } \|z\| < 1, \tag{2.34}$$

[2]Since $\text{div}[\boldsymbol{v}] = 0$, $\text{div}[2\mu_0\boldsymbol{D}] = \mu_0\Delta\boldsymbol{v}$, where $\Delta(\cdot) := \text{div}[\text{grad}(\cdot)]$ is the Laplacian operator.

we obtain a Forcheimmer-like formula for the drag coefficient

$$\boldsymbol{m} \approx [\alpha_0 + \alpha_0\alpha_1\|\boldsymbol{v}_{\text{rel}}\|]\boldsymbol{v}_{\text{rel}} \tag{2.35}$$

In this case, the governing equation, assuming $\mu(p, \hat{\boldsymbol{T}}, \boldsymbol{m}) = \mu_0 > 0$ is:

$$-(\alpha_0\alpha_1\|\boldsymbol{v}\| + \alpha_0)\,\boldsymbol{v} + \text{grad}[p] - \text{div}[2\mu_0\boldsymbol{D}] = \rho\boldsymbol{b}, \tag{2.36a}$$

$$\text{div}[\boldsymbol{v}] = 0. \tag{2.36b}$$

4. By choosing $\mu(p, \hat{\boldsymbol{T}}, \boldsymbol{m}) = \mu_0[1 + \gamma\|\hat{\boldsymbol{T}}\|^2]^n$, we obtain the "stress power law" model,

$$\boldsymbol{D} = \frac{\hat{\boldsymbol{T}}}{2\mu_0[1 + \gamma\|\hat{\boldsymbol{T}}\|^2]^n}, \tag{2.37}$$

which is the counterpart to the classical power law model which can show shear thinning/thickening behaviour. For an extensive discussion of such "stress power law" models, the reader is invited to consult [68].

It appears that it would not be possible to obtain the general form of the classical power law model by starting with the Helmholtz potential as has been done in this study.

It is clear that the generalizations of the Brinkman model have been obtained under the assumptions recorded in Section 2.3 and the special form of the dissipation considered in equation (2.29), namely, that dissipation at the pores and dissipation in the fluid bulk due to shear are both significant.

## 2.6 Generalizations of the Darcy model

If the dissipation due to the drag at the pores is much larger than the dissipation due to shear in the fluid bulk, i.e.,

$$2\mu\|\boldsymbol{D}\|^2 \ll \alpha\|\boldsymbol{v}_{\text{rel}}\|^2, \tag{2.38}$$

then it is reasonable to simplify equation (2.29) to

$$\xi(\boldsymbol{D}, \boldsymbol{v}_{\text{rel}}) \approx \alpha(p, \hat{\boldsymbol{T}}, \boldsymbol{m})\|\boldsymbol{v}_{\text{rel}}\|^2, \text{ where } \alpha > 0. \tag{2.39}$$

Then, from equation (2.23) and equation (2.39), we obtain that

$$\xi(\boldsymbol{D}, \boldsymbol{0}) = 0 = \hat{\boldsymbol{T}} \cdot \boldsymbol{D} \quad \forall \ \text{tr}[\boldsymbol{D}] = 0. \tag{2.40}$$

From equation (2.40), we conclude that $\hat{\boldsymbol{T}}$ must be a scalar multiple of the identity tensor, but since $\hat{\boldsymbol{T}}$ is deviatoric, this implies that $\hat{\boldsymbol{T}} \equiv \boldsymbol{0}$.

Equation equation (2.23) then simplifies to

$$\xi = \boldsymbol{m} \cdot \boldsymbol{v}_{\text{rel}}. \tag{2.41}$$

Now maximizing $\xi(\boldsymbol{v}_{\text{rel}})$ with respect to $\boldsymbol{v}_{\text{rel}}$ with equation (2.41) as the constraint, it is easy to see that we obtain

$$\boldsymbol{T} = -p\boldsymbol{I}, \tag{2.42a}$$

$$\boldsymbol{m} = \alpha(p, \hat{\boldsymbol{T}}, \boldsymbol{m})\boldsymbol{v}_{\text{rel}}. \tag{2.42b}$$

Fixing the frame to the solid as before, we are led to the governing equation:

$$\alpha\boldsymbol{v} + \text{grad}[p] = \rho\boldsymbol{b}, \tag{2.43a}$$

$$\text{div}[\boldsymbol{v}] = 0, \tag{2.43b}$$

which is clearly a generalization of Darcy's model. The various choices for the function $\alpha(p, \hat{\boldsymbol{T}}, \boldsymbol{m})$ mentioned earlier yield different generalizations of Darcy's model.

## 2.7 Conclusion

In this short note, we developed various generalizations of the Brinkman and Darcy models by appealing to a thermodynamic framework that has been used successfully to describe very distinct types of material response using the hypothesis of maximization of the rate of entropy production. Such an approach clarifies some issues that are not apparent in a conventional approach such as the role that the dissipative mechanisms play. The approach allows one to develop systematically, models that are consistent with the laws of thermodynamics by choosing appropriate forms for the Helmholtz potential and the rate of dissipation function.

# 3. FLOW OF A FLUID THROUGH POROUS MEDIA DUE TO HIGH PRESSURE GRADIENTS: PART 1 - STEADY FLOWS*

Darcy's equation [11] is the most popular mathematical model to describe the flow of fluids through a porous solid due to an applied pressure gradient. Darcy's equation, which is commonly referred to as "Darcy's law" is an approximation that is valid only if numerous assumptions are met (See Munaf *et al.* [13], Rajagopal [47]). Far from being a "law" with universal or for that matter wide ranging applicability, the classical Darcy's equation, which is an approximation to the balance of linear momentum is reasonable only if

1. The solid is a rigid porous body whose balance of linear momentum can be ignored. The stresses developed in the rigid solid body being that which is necessary to meet the balance of linear momentum.

2. The pore structure in the solid is uniform and hence there is no inhomogeneity in the pore structure.

3. The flow is sufficiently slow so that the inertial effects in the fluid can be neglected.

4. The frictional effects in the fluid due to the viscosity of the fluid can be neglected.

5. The only interaction between the solid and the fluid is due to the friction at the pores and is proportional to the relative velocity between the solid and the fluid.

6. The flow is steady.

7. The fluid is incompressible.

*Reprinted with permission from Flow of a fluid through a porous solid due to high pressure gradients by Shriram Srinivasan, Andrea Bonito, and K.R. Rajagopal, 2012. *Journal of Porous Media*, 16(3):193–203, Copyright 2012 by Begell House, Inc.

8. The pressure range that the fluid is subject to does not lead to changes in the viscosity of the fluid.

9. The partial stress in the fluid is that in an Euler fluid.

In this section, we are interested in the flow of a fluid through a porous solid when assumptions (4),(8) and (9) do not hold. Such flows have relevance to several problems in petroleum and geotechnical engineering, such as EOR and CS where the range of pressure that the fluid is subject to is very large. In some of the problems, more than one fluid is involved such as steam and oil in EOR. However before embarking on the study of such problems, it is necessary to study the problem of a single fluid flowing through a porous solid. When assumption (4) alone does not hold, we obtain the equations developed by Brinkman [18, 19].

The variation of the viscosity with the pressure implies that the "Drag coefficient" that appears in the equations governing the flow of a liquid through a porous solid will depend on the pressure.

In this study, while we assume that the viscosity and "Drag coefficient" depend on the pressure, we assume that the other assumptions mentioned above hold. This leads to a generalization of the Brinkman equation with the viscosity and the "Drag coefficient" depending upon the pressure. Recently, Nakshatrala and Rajagopal [58] studied the generalization of Darcy's equation when the "Drag coefficient" depends on the pressure.

As we mentioned earlier, Barus [25] suggested an exponential dependence of the viscosity on the pressure, i.e.,

$$\mu(p) = \mu_0 \exp(\beta p), \quad \mu_0 > 0,\ \beta \geq 0, \tag{3.1}$$

where $\mu_0$ and $\beta$ are constants , with $\mu_0$ having the dimension of viscosity and $\beta$ the dimension that is the inverse of that of the pressure. The expression equation (3.1) would

lead to a "Drag coefficient" $\alpha(p)$ of the form

$$\alpha(p) = \alpha_0 \exp(\beta p), \quad \alpha_0 \geq 0, \tag{3.2}$$

where $\alpha_0$ is a constant with dimension of $\mathrm{ML}^{-3}\mathrm{T}^{-1}$.

Using a semi-inverse approach, Kannan and Rajagopal [59] studied the flow of a fluid through a porous inclined slab. They considered a variety of forms for the dependence of viscosity and the "Drag coefficient" including the exponential dependence given in equation (3.1), equation (3.2). We shall not get into a detailed discussion of their results, suffice it is to say the solutions exhibited markedly different characteristics than the solutions for the classical Darcy and Brinkman equations. The semi-inverse solution sought simplifies the problem greatly and the governing equations reduce to a simple ordinary differential equation.

Recently, Nakshatrala and Rajagopal [58] were able to study numerically the problem corresponding to the generalization of Darcy's equation, when the "Drag coefficient" depends exponentially on the pressure as given in equation (3.2). They were able to find solutions to the partial differential equation governing the flow using a mixed finite element method. They showed that the results they obtain are different from the solution to the classical Darcy's equation. Assuming that the "Drag coefficient" is a bounded function of the pressure in the generalized Darcy's equation, Girault *et al.* [69] guaranteed the well-posedness of the system together with the convergence of a finite element method. When the dependence on the pressure is exponential (as in equation (3.2)), the authors propose an interesting splitting algorithm, observed numerically to be robust in the parameter range tested.

The generalization of the Brinkman equation considered here (viscosity and "Drag coefficient" given by equation (3.1) and equation (3.2) respectively), no theoretical convergence results are available. While we are unable to obtain a numerical solution of the governing equations for large values of the non-dimensionalized pressure-viscosity coefficient "$\beta$" that

appears in the viscosity-pressure relation equation (3.1) , we are however able to obtain solutions to the problem when the non-dimensionalized pressure-viscosity coefficient $\bar{\beta}$ is small. Fortunately, for the class of incompressible fluids (like mineral oil for instance) that we are interested in, the non-dimensionalized pressure-viscosity coefficient $\bar{\beta}$ is indeed small (see Section 3.3 for details).

It is worth noting that the viscosity data for various pressures have been obtained from experiments where the applied pressure is positive, i.e., the applied normal stress is compressive. When the pressure is sufficiently low cavitation can occur, leading to the formation of cavities or bubbles in the flow field. Cavitation is the phenomenon that occurs at sufficiently low pressure, when the pressure of the fluid at the location becomes less than the vapor pressure of the liquid at that temperature at the location in question. Cavitation occurs in the flows of fluids through pumps, bearings and adjacent to rotating propellers amongst other flows. The "Drag" due to the motion of a solid in a cavitating fluid is not well understood and more importantly there is no measurement of the viscosity of fluids in such a state. In view of this, we shall adopt a procedure that is followed in lubrication and assume that when the pressure becomes negative the viscosity corresponds to that for zero pressure (see Szeri [70] for a detailed discussion of the manner in which cavitation is handled within the context of obtaining numerical solutions in elastohydrodynamics wherein very high pressures are involved). For the fluids considered here, we shall assume that the variation of viscosity and "Drag coefficient" is negligible when the pressure is negative and that both the viscosity and "Drag coefficient" are a continuous function of the pressure. Furthermore, the numerical method used requires that the function be differentiable. In Appendix A the viscosity and "Drag coefficients" are chosen to be a particular smooth function of the pressure which satisfies all our hypotheses.

When $\beta = 0$, the problem reduces to that considered by Brinkman, namely the viscosity being constant.

When the viscosity and "Drag coefficient" is given by equation (3.1) and equation (3.2) respectively, we find that the volumetric flux due to the pressure gradient is distinctively

and characteristically different. While the classical Brinkman equation predicts a linear relationship between the volumetric flux and the pressure gradient as the pressure gradient increases, the model employed in the study predicts a ceiling flux as the pressure gradient increases. One would expect such a relationship as one cannot push through more than a certain quantity of fluid. In fact, increasing the pressure gradient significantly will lead to the flow becoming turbulent with the possibility of back flow, leading in fact to the diminishing of the volumetric flux at very high pressure gradient. As is to be expected, we also find that as the pressure difference between the inlet and the outlet increases, the region wherein the component of the velocity is close to a constant decreases, that is, the effect of the no-slip velocity boundary condition is more pronounced when the pressure gradient causing the flow is larger. We also find that the component of the velocity in the direction normal to the gradient (see Figure 3.1) increases when the pressure gradient increases.

The organization of the section is as follows: In Section 3.1 we introduce the problem and record the governing equations and the boundary conditions. In Section 3.2, we derive the non-dimensional equations that govern the flow, and this is followed by Section 3.3 where we discuss the numerical solution to the problem on hand and make some concluding remarks. A brief description of the finite element scheme used for the computational resolution of the problem is given in Appendix A.

## 3.1 Governing equations

The assumption that the viscosity of the fluid depends on the pressure and that the frictional effects in the fluid are not ignored implies that the Cauchy stress $\boldsymbol{T}$ in the fluid is given by

$$\boldsymbol{T} = -p\mathbf{1} + 2\mu(p)\boldsymbol{D}, \tag{3.3}$$

where $-p\mathbf{1}$ is the indeterminate part of the stress due to the constraint of incompressibility, $\boldsymbol{v}$ is the velocity of the fluid, $\mu(p)$ is the pressure dependent viscosity and $\boldsymbol{D}$ denotes the

symmetric part of the velocity gradient, i.e.,

$$\boldsymbol{D} := \frac{1}{2}\left[\left(\frac{\partial \boldsymbol{v}}{\partial \boldsymbol{x}}\right) + \left(\frac{\partial \boldsymbol{v}}{\partial \boldsymbol{x}}\right)^{T}\right]. \tag{3.4}$$

The balance of linear momentum for the fluid, on neglecting body forces, is given by

$$\rho \frac{d\boldsymbol{v}}{dt} = \operatorname{div}[\boldsymbol{T}] + \boldsymbol{I}, \tag{3.5}$$

where $\boldsymbol{I}$ is the interaction between the solid and the fluid, namely the frictional resistance at the pores of the solid on the fluid that is flowing.

In general, there could be various other interaction mechanisms: drag, virtual mass effect, Magnus effect, Basset forces, Faxen forces, density gradient effects, temperature gradient effects, etc. We shall assume that the only interaction mechanism is that due to drag and that $\boldsymbol{I}$ is given by

$$\boldsymbol{I} = -\alpha(p)\boldsymbol{v}. \tag{3.6}$$

Since we shall be interested in slow flow, inertial effects in equation (3.5) are neglected. Also, since we shall assume that the fluid is incompressible, the velocity field has to satisfy the constraint that

$$\operatorname{div}[\boldsymbol{v}] = 0. \tag{3.7}$$

It follows from equation (3.3)–equation (3.6), on neglecting the inertial term that the appropriate governing equation is

$$-\frac{\partial p}{\partial \boldsymbol{x}} + \operatorname{div}[2\mu(p)\boldsymbol{D}] - \alpha(p)\boldsymbol{v} = \boldsymbol{0}. \tag{3.8}$$

We shall be interested in the flow in a slab [1] due to the applied tractions on the surfaces

[1] A similar problem was studied by Subramanian and Rajagopal [71]. However a semi-inverse method was employed in that study which simplified the problem to a unidirectional flow across the slab. Here, we solve the system of partial differential equations that allows for flow along the direction of the pressure gradient as well as normal to it.

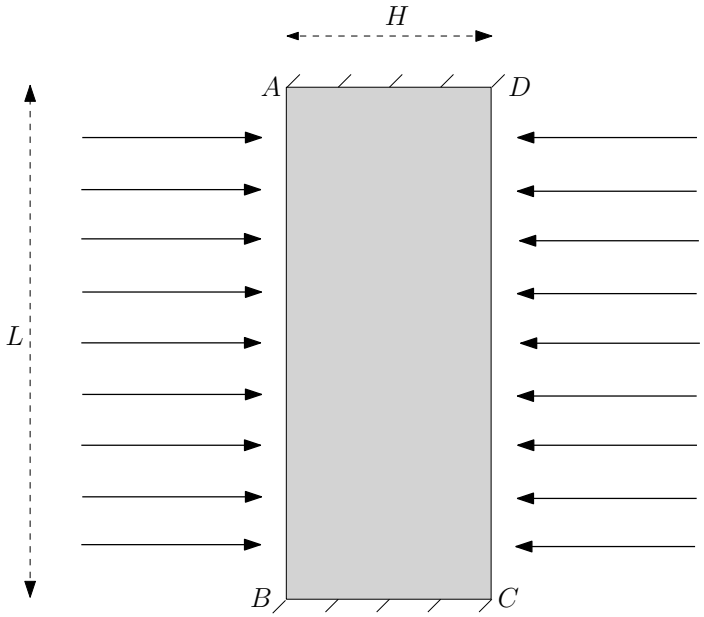


Figure 3.1: Pressure driven flow through a slab of length $L$ and width $H$. A purely normal traction is applied at the left and right boundaries. The fluid satisfies no-slip boundary condition at the top and bottom of the slab.

$AB$ and $CD$, that is,

$$\boldsymbol{t}\Big|_{AB} = [-p\mathbf{1} + 2\mu(p)\boldsymbol{D}]\Big|_{AB}\boldsymbol{n}_{AB}, \tag{3.9a}$$

$$\boldsymbol{t}\Big|_{CD} = [-p\mathbf{1} + 2\mu(p)\boldsymbol{D}]\Big|_{CD}\boldsymbol{n}_{CD}, \tag{3.9b}$$

where $\boldsymbol{n}_{AB}$ and $\boldsymbol{n}_{CD}$ denote the outward unit normals on the surface $AB$ and $CD$ (see Figure 3.1). It is important to recognize that the traction boundary conditions not only take into account the appropriate pressure, they also take into account the appropriate components of the velocity gradient. In addition to the above boundary conditions on the surface $AB$ and $CD$, we assume that on the surface $BC$ and $AD$, the fluid satisfies the no-slip boundary condition, i.e.,

$$\boldsymbol{v}\Big|_{BC} = \boldsymbol{v}\Big|_{AD} = \mathbf{0}. \tag{3.10}$$

Thus we need to solve equation (3.8) subject to the boundary conditions equation (3.9) and equation (3.10).

It must be remembered that classical solutions are not possible even in the case of linear partial differential equations unless the boundary data satisfy certain compatibility conditions (see [72]). Such is the case in the present work, for the chosen values of the applied traction on $AB$ and $CD$ lead to an incompatibility at the corners. This leads to sharp gradients and concomitant numerical difficulties in solving the discretized system of non-linear algebraic equations and the incompatibility of the boundary conditions leads to singularity at the boundary that leads to the spike in the pressure that is observed in the numerical solution that we have obtained.

It is worth observing that when the viscosity and the "Drag coefficient" are independent of the pressure, we recover the classical Brinkman equation. If the frictional effects within the fluid are ignored, we obtain the equations considered by Nakshatrala and Rajagopal [58], which is the generalization of Darcy's equation for a pressure dependent "Drag coefficient" . Equation equation (3.8) can be generalized to

$$-\frac{\partial p}{\partial \boldsymbol{x}} + \operatorname{div}[2\mu(p)\boldsymbol{D}] - \alpha(\|\boldsymbol{v}\|)\boldsymbol{v} = \boldsymbol{0}, \tag{3.11}$$

which is the generalization of equation (3.8) to include a Forchheimer like term (see Forchheimer [17]). A generalization of the Brinkman model to describe power law fluids has been considered in [73] and [74].

## 3.2 Non-dimensional equations

In order to carry out a systematic study we shall appropriately non-dimensionalize the governing equations. Let us suppose that the surface $CD$ is exposed to the atmosphere so that the pressure (the mean normal stress) is the atmospheric pressure $p_0$. We introduce

the following non-dimensionalization

$$\bar{p} := \frac{p}{p_0},\ \bar{\boldsymbol{x}} := \frac{\boldsymbol{x}}{H},\ \bar{\beta} := \frac{\beta}{\frac{1}{p_0}},\ \bar{\boldsymbol{v}} := \frac{\boldsymbol{v}}{v_0}, \tag{3.12}$$

where $H$ is the thickness of the slab (see Figure 3.1) and $v_0$ is a representative velocity, say

$$v_0 := \frac{p_0}{\alpha_0 H}. \tag{3.13}$$

Also, let

$$\bar{\mu} := \frac{\mu}{\mu_0},\ \bar{\alpha} := \frac{\alpha}{\alpha_0}. \tag{3.14}$$

The following non-dimensional counterpart of equation (3.1)

$$\bar{\mu}(\bar{p}) = \bar{\alpha}(\bar{p}) = \begin{cases} \exp(\bar{\beta}\bar{p}) & \text{if } \bar{p} > 0, \\ 1 & \text{if } \bar{p} \leq 0, \end{cases} \tag{3.15}$$

is evidently a continuous function of the pressure. However, the function in equation (3.15) is not differentiable in the classical sense, and we postpone to Appendix A the description of the numerical method.

It follows from equation (3.12)–equation (3.15) that equation (3.8) can be expressed as

$$-\bar{\text{grad}}[\bar{p}] - \bar{\alpha}(\bar{p})\bar{\boldsymbol{v}} + \frac{1}{\mathcal{A}}\bar{\text{div}}[2\bar{\mu}(\bar{p})\bar{\boldsymbol{D}}] = \boldsymbol{0}, \tag{3.16a}$$

$$\bar{\text{div}}[\bar{\boldsymbol{v}}] = 0, \tag{3.16b}$$

where $\bar{\text{grad}}[\cdot] := \dfrac{\partial(\cdot)}{\partial\bar{\boldsymbol{x}}}$, $\bar{\text{div}}[\cdot] := \text{tr}[\bar{\text{grad}}[\cdot]]$, $\bar{\boldsymbol{D}} := \dfrac{1}{2}\left[\left(\dfrac{\partial\bar{\boldsymbol{v}}}{\partial\bar{\boldsymbol{x}}}\right) + \left(\dfrac{\partial\bar{\boldsymbol{v}}}{\partial\bar{\boldsymbol{x}}}\right)^T\right]$ and $\mathcal{A} := \dfrac{\alpha_0 H^2}{\mu_0}$ is a non-dimensional number that is the ratio of the frictional effect due to drag (frictional effect between the fluid and the pores in the solid) to the frictional effect within the fluid due to viscosity. We shall also find it convenient to introduce two additional non-dimensional

numbers

$$\gamma := \frac{L}{H}, \quad P := \frac{p_{AB}}{p_0}. \tag{3.17}$$

The non-dimensional forms of the traction boundary conditions are then

$$\bar{\boldsymbol{t}}\Big|_{\bar{x}=1} = -1\mathbf{i}, \tag{3.18a}$$

$$\bar{\boldsymbol{t}}\Big|_{\bar{x}=0} = P\mathbf{i}, \tag{3.18b}$$

while the corresponding non-dimensional form of the no-slip boundary condition is

$$\bar{\boldsymbol{v}}\Big|_{\bar{y}=0} = \bar{\boldsymbol{v}}\Big|_{\bar{y}=\gamma} = \mathbf{0}. \tag{3.19}$$

The domain and the boundary conditions for equation (3.16) that we shall work with are illustrated in Figure 3.2.

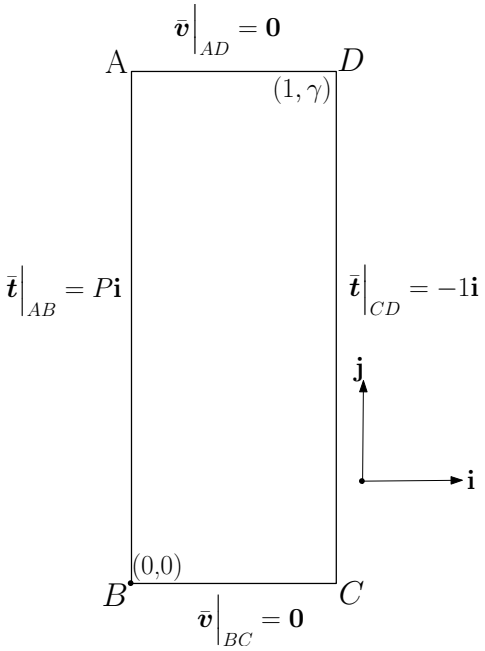


Figure 3.2: Pressure driven flow through a slab of length $\gamma$ and width 1 with boundary conditions indicated on all sides of the slab.

Thus we solve equation (3.16) with the form for $\bar{\mu}, \bar{\alpha}$ given by equation (3.15) subject to the boundary conditions equation (3.18) and equation (3.19).

## 3.3 Numerical results

The various parameters in the problem were chosen as follows: We let $\alpha_0 = \mu_0 = 1$ and set $H = 1, L = 10$. This in conjunction with $p_0 = 10^5$ yields $\gamma = 10$, $\mathcal{A} = 1$. The traction at the left end is varied by varying $P$. From the experiments reported in [43, 42, 44] the measured value of the reciprocal of the pressure-viscosity exponent $\beta$ is seen to lie in the range 30 MPa to 100 MPa for the fluids measured. Hence we choose to study the cases $\beta =$ 0, $1 \times 10^{-8}$, $2 \times 10^{-8}$, $3 \times 10^{-8}$ and $3.5 \times 10^{-8}$ (in units of $\mathrm{Pa}^{-1}$) which give a qualitative picture of the effects of pressure dependent viscosity over the range of measured values of the exponent $\beta$. The case $\beta = 0$ corresponds to the case of constant viscosity (or the standard Brinkman model). The values chosen for $\beta$ lead to values of $\bar{\beta} = 0$, $1 \times 10^{-3}$, $2 \times 10^{-3}$, $3 \times 10^{-3}$ and $3.5 \times 10^{-3}$. We allow $P$ to take on the values 1, 100, 200, 300, 400 and 500.

Note that the traction is specified at $\bar{x} = 0$ and $\bar{x} = 1$ and no-slip boundary condition is enforced at $\bar{y} = 0$ and $\bar{y} = 10$ including the corners.

We shall find it convenient to represent $\bar{\boldsymbol{v}}$ as

$$\bar{\boldsymbol{v}} = \bar{V}_x \mathbf{i} + \bar{V}_y \mathbf{j}. \tag{3.20}$$

A quantity of interest in this problem is the flux or flow rate obtained at the end of the slab that is open to the atmosphere, i.e., the side $CD$. We denote the non-dimensional flux by $\bar{q}$, where

$$\bar{q} := \int_{CD} [\bar{\boldsymbol{v}} \cdot \boldsymbol{n}_{CD}] \, \mathrm{d}l = \int_0^{\gamma} \bar{V}_x(1, \bar{y}) \mathrm{d}\bar{y}. \tag{3.21}$$

The system of (non-dimensionalized) partial differential equations equation (3.16) with the form for $\bar{\mu}, \bar{\alpha}$ given by equation (A.3) subject to the boundary conditions equation (3.18) and equation (3.19) was solved using a mixed finite element method, details of which are

provided in the Appendix A.

The profiles of $\bar{V}_x$ and $\bar{p}$ at AB are shown in Figure 3.3 while the profiles at CD are shown in Figure 3.4. The lack of smoothness near the corners is expected; there is an incompatibility at the corners due to the change from the specified value of traction at AB and CD to a no-slip boundary condition at BC and AD. One can also notice that the velocity for the constant viscosity case is almost 200 % more than that for the variable viscosity case

The contours of velocity and pressure over the entire domain are indicated in Figure 3.5. The contours of $\bar{V}_y$ indicate that unidirectional flow occurs only in a small region close to the middle of the slab. The pressure does not vary too much over the domain except for the occurrence of high pressures at some points close to the boundaries.

The variation of flux for different forcing pressures is shown in Figure 3.6. This is of great import because one observes that a standard Brinkman model with constant viscosity grossly overpredicts the flux; by as much as almost 250 % for a pressure difference across the slab equal to 499 (which occurs when $P = 500$); the over prediction increases nearly linearly as can be seen from the figure. Also, the figure indicates that for the value of $\bar{\beta} = 3.5 \times 10^{-3}$, there is very negligible increase in the flux for forcing pressures $P > 200$ , that is there seems to be a ceiling flux as is to be expected on physical grounds. This is in direct contrast to the case where the viscosity is constant and the model predicts a flux that will increase continuously with increase in $P$.

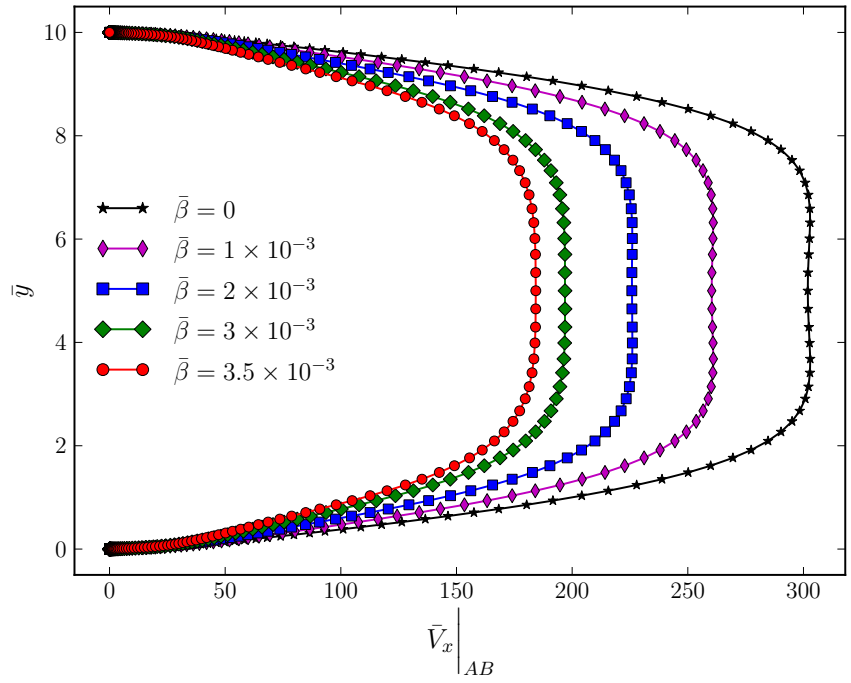


(a)

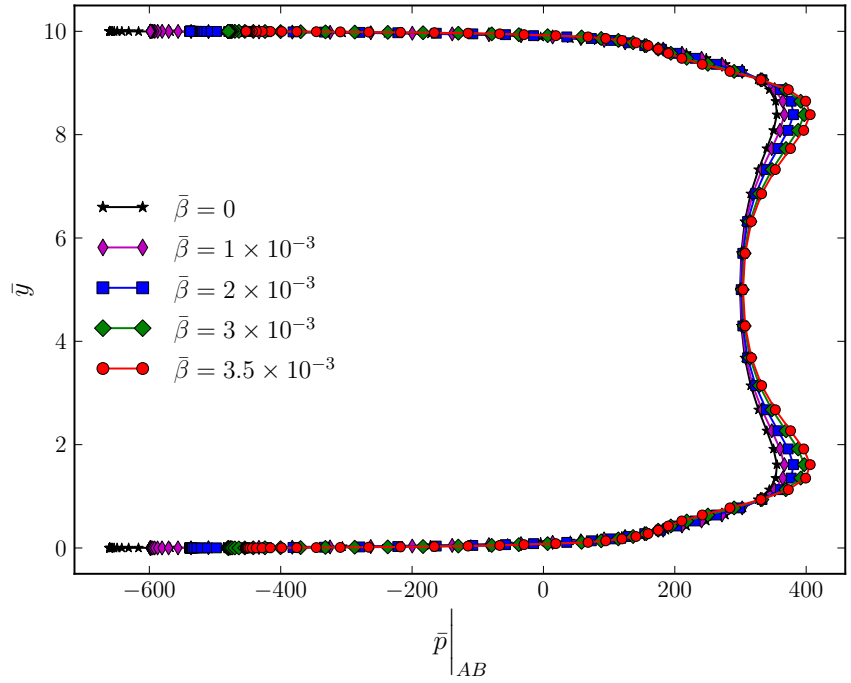


(b)

Figure 3.3: Velocity and pressure profiles at the left end $\bar{x} = 0$ with $P = 300$ for various $\bar{\beta}$.

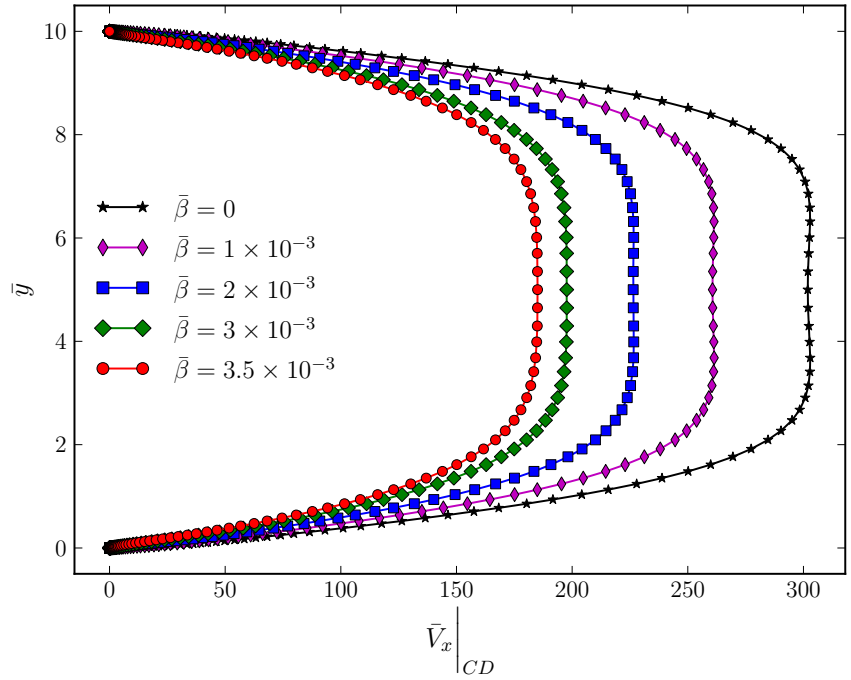


(a)

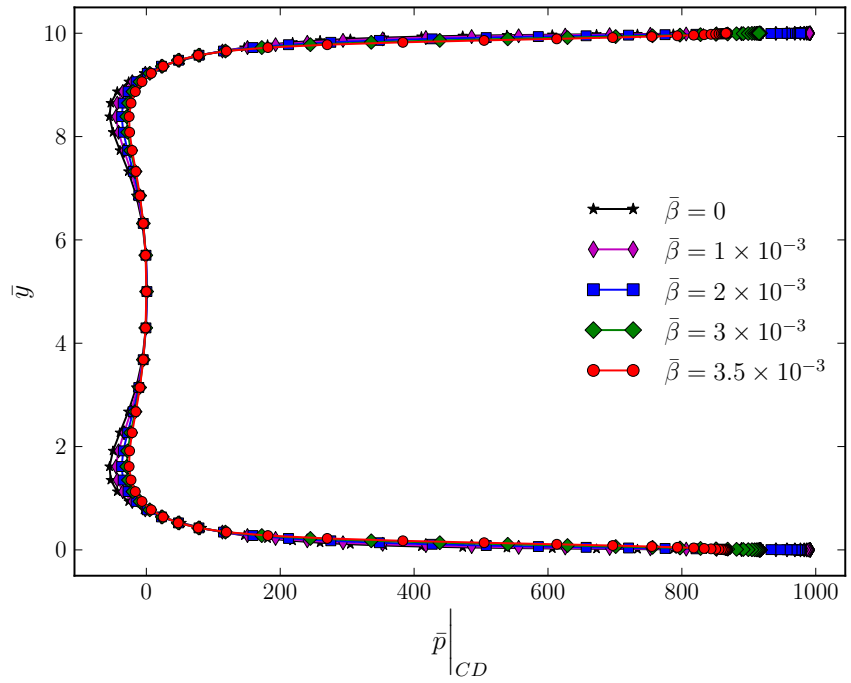


(b)

Figure 3.4: Velocity and pressure profiles at the right end $\bar{x} = 1$ with $P = 300$ for various $\bar{\beta}$.

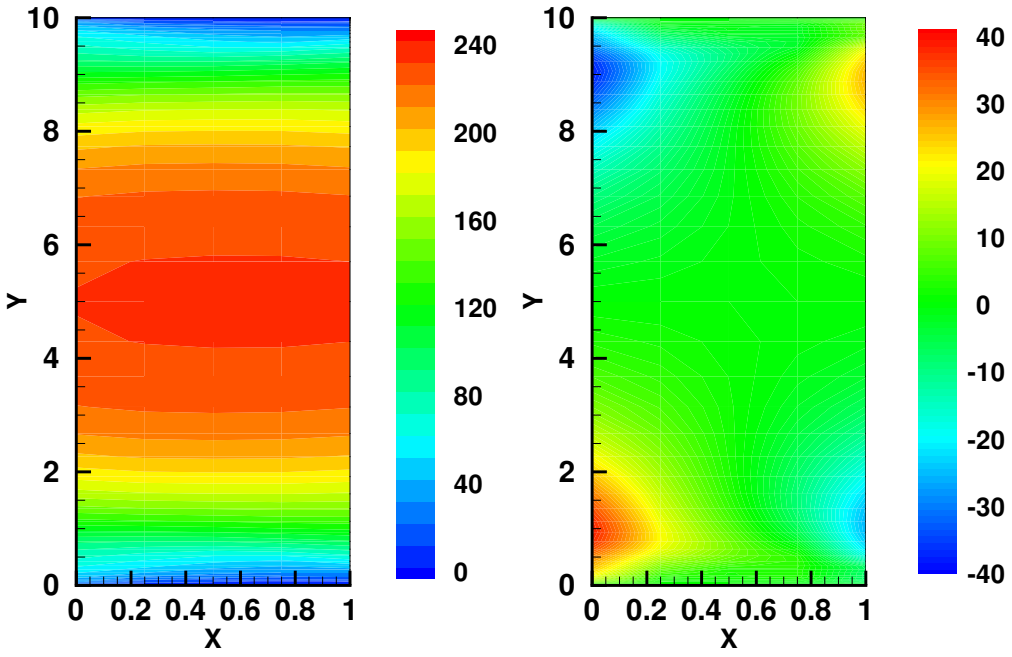


(a) $\bar{V}_x$ (b) $\bar{V}_y$

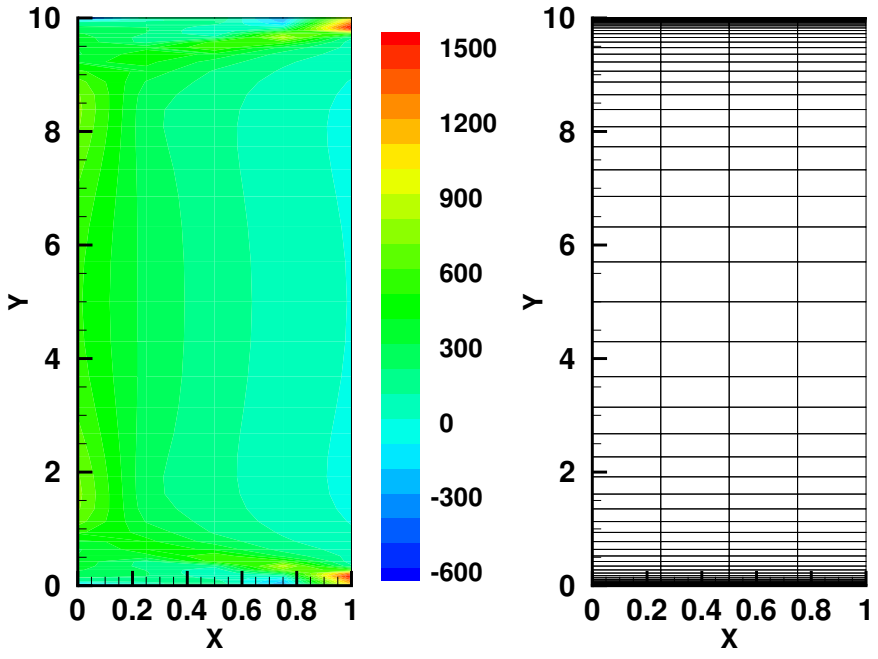


(c) $\bar{p}$ (d)

Figure 3.5: Contours of velocity and pressure for $\bar{\beta} = 3.5 \times 10^{-3}$ when $P = 500$. The finite element mesh used is also shown.

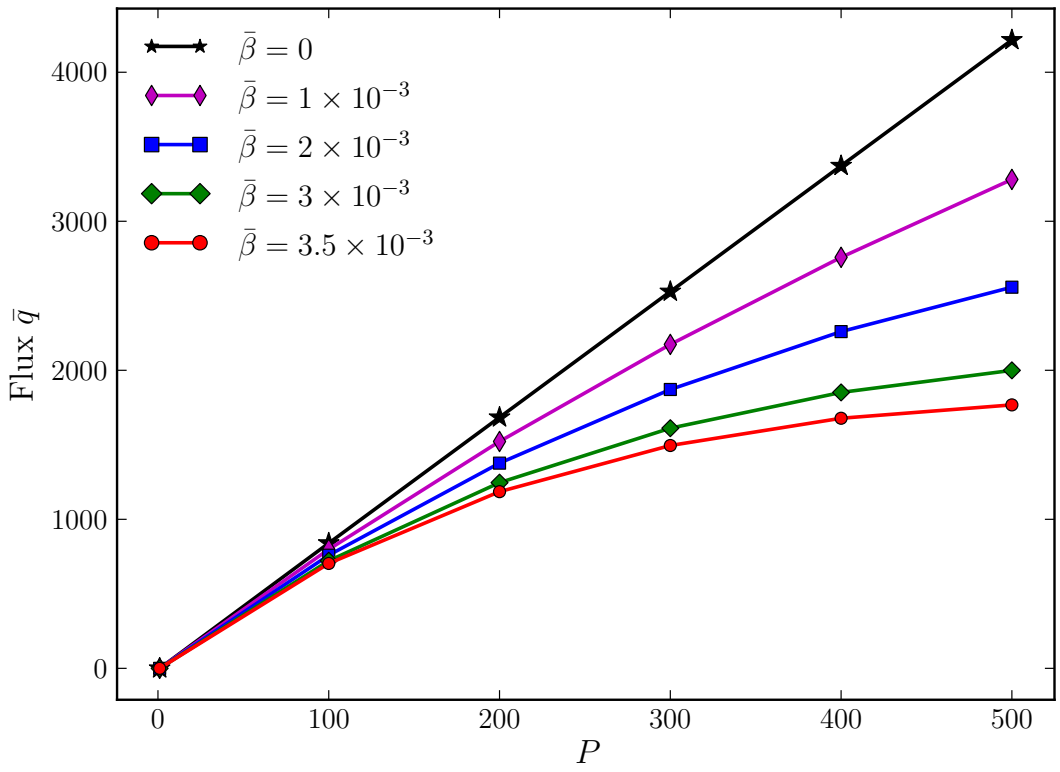


Figure 3.6: Flow rate through slab for different values of traction at the left boundary.

# 4. FLOW THROUGH A HETEROGENEOUS POROUS MEDIUM

## 4.1 Motivation

In our study thus far, it has been assumed that the pore structure of the porous solid is uniform, and its permeability to flow is the same in all directions, i.e., the porous medium may be said to be homogeneous and isotropic with regard to its permeability. Thus the *permeability* $k$ was assumed to be a constant scalar. This is not true in general, a porous medium may be heterogeneous, for example a bed of silt could be interspersed with inclusions of clay, sand or solid rock in which case the permeability to flow changes not only with spatial location but direction as well.

In such cases the *permeability* is described by a second order tensor $\boldsymbol{K}(\boldsymbol{x})$ which is symmetric and positive definite [75]. Thus it is invertible and the "drag coefficient" is now represented by a positive definite, symmetric, second order tensor $\boldsymbol{\Lambda} = \mu \boldsymbol{K}^{-1}(\boldsymbol{x})$. The positive definiteness of $\boldsymbol{\Lambda}$ is necessary and sufficient to ensure that the rate of entropy production is non-negative and thus automatically meet the second law of thermodynamics. This becomes clear on examining equation (2.29), where the term $\alpha(p, \hat{\boldsymbol{T}}, \boldsymbol{m})\|\boldsymbol{v}_{\text{rel}}\|^2$ modified to $\boldsymbol{\Lambda}(p, \hat{\boldsymbol{T}}, \boldsymbol{m})\boldsymbol{v}_{\text{rel}} \cdot \boldsymbol{v}_{\text{rel}}$ is non-negative by the very definition of positive definiteness of a second order tensor. In fact the derivation carried out in Section 2 , with the minor modification made above leads to an identical result with $\boldsymbol{\Lambda}$ in place of $\alpha$. When the medium is isotropic, the permeability tensor reduces to a spherical tensor and we recover the scalar form.

When the viscosity depends on the pressure, we can express the drag coefficient as

$$\boldsymbol{\Lambda} = \boldsymbol{\Lambda}_0(\boldsymbol{x}) \exp(\beta p) \tag{4.1}$$

analogous to equation (3.2) in Section 3.

## 4.2 Problem definition and governing equations

We shall consider a slight modification of the problem considered in the last section, namely, the porous medium is now assumed to be inhomogeneous and anisotropic. The solid is assumed to contain an inclusion whose permeability is different from that of the medium. However, all other assumptions remain the same. We shall consider three problems with inhomogeneities of different geometries illustrated by Figure 4.1.

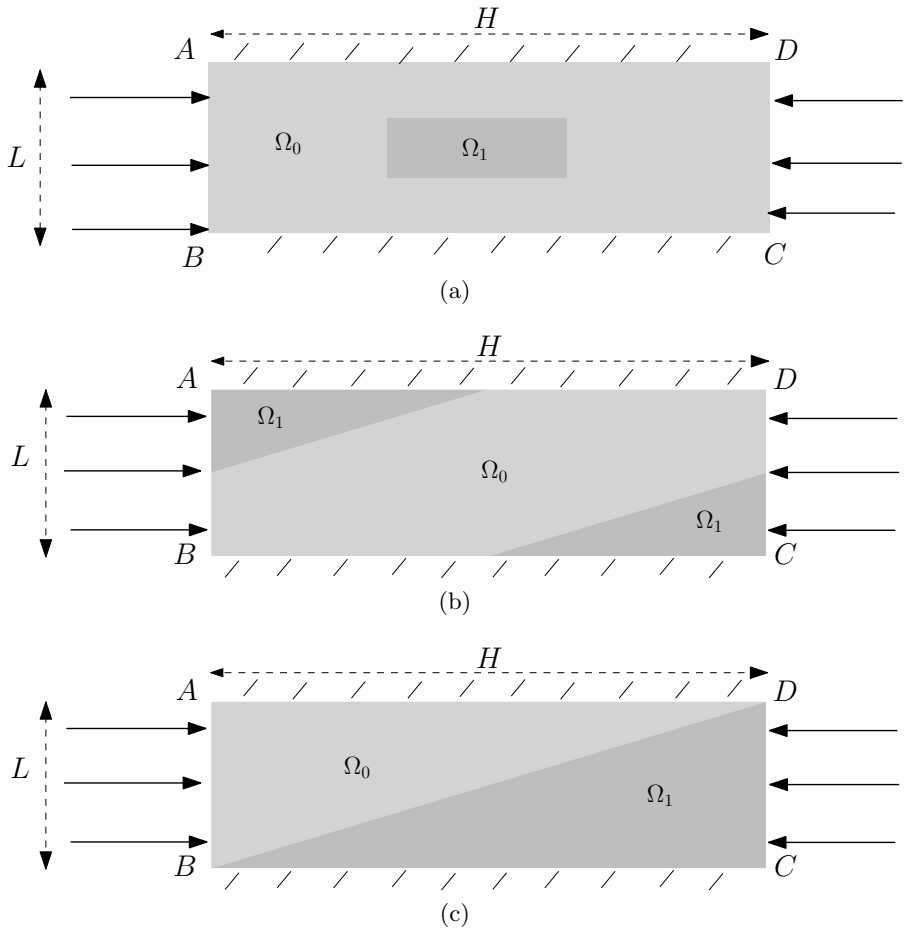


Figure 4.1: Pressure driven flow through a heterogeneous rigid slab of length $L$ and width $H$. A purely normal traction is applied at the left and right boundaries. The fluid satisfies no-slip boundary condition at the top and bottom of the slab. The subdomain $\Omega_0$ is assumed to be homogeneous and isotropic unless mentioned otherwise.

The governing equations are non-dimensionalized using the scheme equation (3.12) as before and they lead to:

$$-\bar{\text{grad}}[\bar{p}] - \bar{\mathbf{\Lambda}}(\bar{p}, \boldsymbol{x})\bar{\boldsymbol{v}} + \frac{1}{\mathcal{A}}\bar{\text{div}}[2\bar{\mu}(\bar{p})\bar{\boldsymbol{D}}] = \mathbf{0}, \tag{4.2a}$$

$$\bar{\text{div}}[\bar{\boldsymbol{v}}] = 0, \tag{4.2b}$$

where

$$\bar{\mathbf{\Lambda}}(\bar{p}, \bar{\boldsymbol{x}}) := \frac{\mathbf{\Lambda}}{\alpha_0} = \frac{\bar{\mathbf{\Lambda}}_0}{\alpha_0}\exp(\bar{\beta}\bar{p}) = \bar{\mathbf{\Lambda}}_0(\bar{\boldsymbol{x}})\exp(\bar{\beta}\bar{p}) \tag{4.3}$$

while the boundary conditions are again

$$\bar{\boldsymbol{t}}\Big|_{\bar{x}=1} = -1\mathbf{i}, \tag{4.4a}$$

$$\bar{\boldsymbol{t}}\Big|_{\bar{x}=0} = P\mathbf{i}, \tag{4.4b}$$

while the corresponding non-dimensional form of the no-slip boundary condition is

$$\bar{\boldsymbol{v}}\Big|_{\bar{y}=0} = \bar{\boldsymbol{v}}\Big|_{\bar{y}=\gamma} = \mathbf{0}. \tag{4.5}$$

## 4.3 Numerical results and discussion

The solution was obtained for $\bar{\beta}$ =0, $2\times10^{-3}$ and $4\times10^{-3}$ while $\gamma = 0.3$, $P = 300$, $\mathcal{A} = 100$ and different cases of $\bar{\mathbf{\Lambda}}_0(\bar{\boldsymbol{x}})$ were considered which are described next. While the same numerical technique (see Appendix A) is used, one needs to generate the mesh for the finite element technique carefully. The elements of the mesh (triangles or quadrilaterals) are permitted to intersect the subdomain interface either at a node or an edge, i.e., each element must lie entirely in subdomain $\Omega_0$ or $\Omega_1$.

The inhomogeneity or anisotropy is due to the term $\bar{\mathbf{\Lambda}}_0(\bar{\boldsymbol{x}})$ which could take on different values at different locations. We shall assume that the subdomain $\Omega_0$ is homogeneous and isotropic with respect to its permeability, and that $\bar{\mathbf{\Lambda}}_0(\bar{\boldsymbol{x}}) = 1$ in $\Omega_0$ unless mentioned

otherwise and consider the following possibilities: A less permeable material specified by the notation $\bar{\mathbf{\Lambda}}_0(\Omega_1) = 1000$ which represents

$$\bar{\mathbf{\Lambda}}_0(\bar{\boldsymbol{x}}) = \begin{cases} 1 \; \forall \; \bar{\boldsymbol{x}} \; \in \; \Omega_0 \\ \\ 1000 \; \forall \; \bar{\boldsymbol{x}} \; \in \; \Omega_1 \end{cases} \tag{4.6}$$

A more permeable material specified by the notation $\bar{\mathbf{\Lambda}}_0(\Omega_1) = \frac{1}{1000}$

$$\bar{\mathbf{\Lambda}}_0(\bar{\boldsymbol{x}}) = \begin{cases} 1 \; \forall \; \bar{\boldsymbol{x}} \; \in \; \Omega_0 \\ \\ \frac{1}{1000} \; \forall \; \bar{\boldsymbol{x}} \; \in \; \Omega_1 \end{cases} \tag{4.7}$$

An anisotropic material specified by listing the characteristic (or eigen) directions and (eigen) values explicitly. For example, with characteristic directions at $\pm 45^\circ$ with side $BC$, and values 1000 and 1,

$$\bar{\mathbf{\Lambda}}_0(\bar{\boldsymbol{x}}) = \begin{cases} 1 \; \forall \; \bar{\boldsymbol{x}} \; \in \; \Omega_0 \\ \begin{pmatrix} 50.05 & 49.95 \\ \\ 49.95 & 50.05 \end{pmatrix} \; \forall \; \bar{\boldsymbol{x}} \; \in \; \Omega_1 \end{cases} \tag{4.8}$$

This representation follows due to the fact that with respect to a basis consisting of the eigen vectors, the matrix associated with the tensor has a diagonal form with entries corresponding to the respective eigen values, and hence changing the basis to the natural basis (unit vectors along the length and width of the slab) yields the matrix representation quoted above. This is the method used to write down matrix representations of the drag coefficient for each case of anisotropy considered here. Subsequently, we shall only mention the characteristic value corresponding to one eigen direction, with the understanding that the second eigen direction (which is normal to the first) shall have a corresponding eigen value of unity.

It is emphasized that a jump in permeability of this magnitude is quite normal in

practice.

For subsequent use, we document that if the eigen value corresponding to the eigen direction *along* diagonal $BD$ be 1000, then

$$\bar{\mathbf{\Lambda}}_0(\bar{\boldsymbol{x}}) = \begin{cases} 1 \; \forall \; \bar{\boldsymbol{x}} \; \in \; \Omega_0 \\ \begin{pmatrix} 917.5 & 274.9 \\ 274.9 & 83.4 \end{pmatrix} \; \forall \; \bar{\boldsymbol{x}} \; \in \; \Omega_1 \end{cases} \tag{4.9}$$

If the eigenvalue corresponding to the eigen direction *normal* to diagonal $BD$ be 1000, then

$$\bar{\mathbf{\Lambda}}_0(\bar{\boldsymbol{x}}) = \begin{cases} 1 \; \forall \; \bar{\boldsymbol{x}} \; \in \; \Omega_0 \\ \begin{pmatrix} 83.4 & -274.9 \\ -274.9 & 917.5 \end{pmatrix} \; \forall \; \bar{\boldsymbol{x}} \; \in \; \Omega_1 \end{cases} \tag{4.10}$$

It would be interesting to see the how the flow field changes due to the heterogeneous inclusion in the medium. One would also like to observe the effect that the inclusion has on the flow rate. It is expected that a more permeable inclusion (lesser value of drag coefficient) will increase the flux while the less permeable inclusion will decrease the flow rate, but it is of greater interest to investigate if the inclusions affect the flow rate to a similar degree.

One answer follows readily from Table 4.1. It is seen that while a more permeable inclusion raises the flow rate by a small amount, a less permeable inclusion decreases the flow rate by a large factor. Secondly, this effect seems to be independent of the pressure viscosity coefficient $\bar{\beta}$.

The streamlines of the flow are shown in Figures 4.2 – 4.4. The homogeneous case has not been shown because it is almost identical (qualitatively) to the case when the inclusion corresponds to a more permeable material. When the inclusion is less permeable than the surroundings, one can see the dramatic changes in the streamlines as they bend around the region of low permeability in Figure 4.2b. In the case of the anisotropic inclusion in

Figure 4.2f, the streamlines follow the direction of more permeability. As expected, in each instance the flow is slower when $\bar{\beta} = 0.004$.

Since the pressure-viscosity exponent $\bar{\beta}$ does not seem to have any new qualitative effect, we exhibit only the case of $\bar{\beta} = 0$ for the other geometries in Figure 4.3 and Figure 4.4. We consider various possibilities of anisotropic behaviour including the case wherein both the subdomains are anisotropic with different eigen values but the same characteristic directions in Figure 4.3f. Whenever the permeability in the flow direction increases, as in Figures 4.2b, 4.3b and 4.4b the streamlines do not show any remarkable change. However, if the subdomain ahead is less permeable as in Figures 4.3c and 4.4c, the streamlines travel normal to the interface between the subdomains.

Table 4.1: Volumetric flux for various cases. The percent change relative to the homogeneous case is also tabulated.

| $\bar{\beta}$ | Homogeneous | $\bar{\mathbf{\Lambda}}_0(\Omega_1) = \frac{1}{1000}$ | % | $\bar{\mathbf{\Lambda}}_0(\Omega_1) = 1000$ | % |
|---|---|---|---|---|---|
| $\bar{\beta} = 0$ | 36.07 | 39.75 | 10.20 | 9.95 | -72.41 |
| | | | | | |
| $\bar{\beta} = 0.002$ | 27.09 | 29.85 | 10.19 | 7.46 | -72.46 |
| | | | | | |
| $\bar{\beta} = 0.004$ | 20.93 | 23.06 | 10.18 | 5.75 | -72.53 |
| | | | | | |

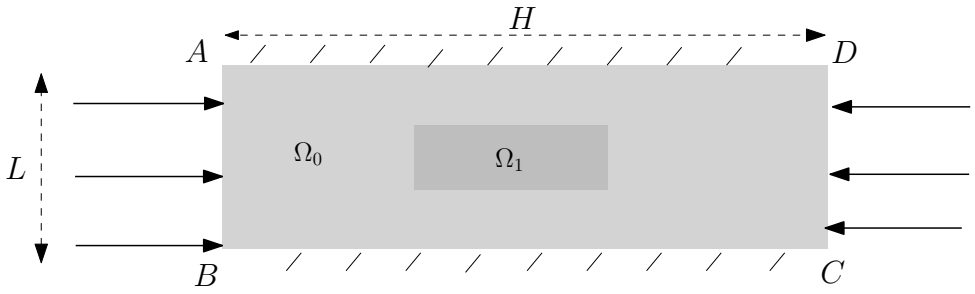


(a)

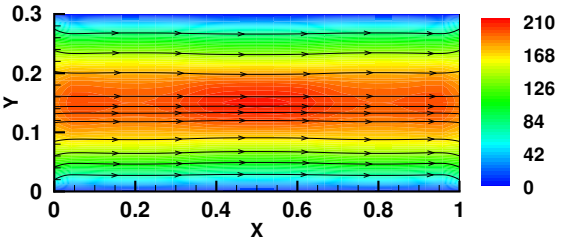


(b) $\bar{\mathbf{\Lambda}}_0(\Omega_1) = \frac{1}{1000}$

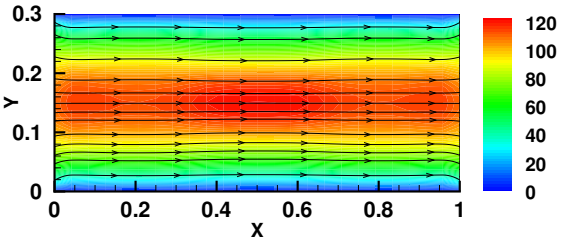


(c) $\bar{\mathbf{\Lambda}}_0(\Omega_1) = \frac{1}{1000}$

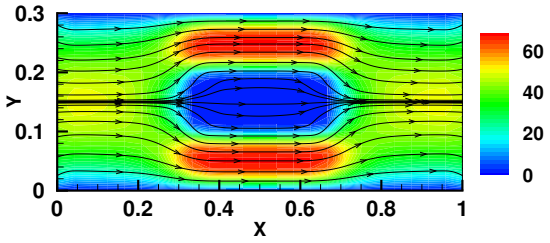


(d) $\bar{\mathbf{\Lambda}}_0(\Omega_1) = 1000$

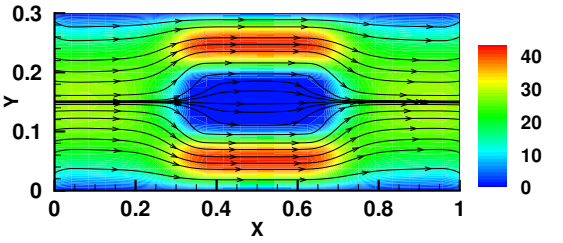


(e) $\bar{\mathbf{\Lambda}}_0(\Omega_1) = 1000$

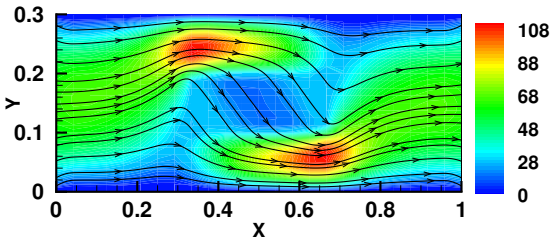


(f) $\Omega_1$ anisotropic

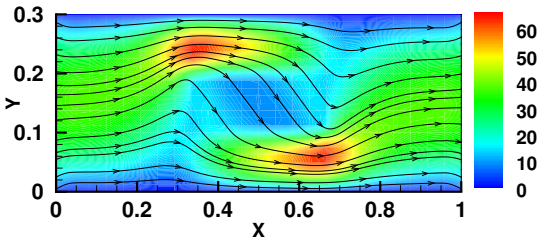


(g) $\Omega_1$ anisotropic

Figure 4.2: The streamlines of the flow field and the contours of the velocity component along the flow direction are shown for different permeability characteristics of the subdomain $\Omega_1$. The figures on the left are those for $\bar{\beta} = 0$ while those on the right are for $\bar{\beta} = 0.004$. The anisotropic medium has an eigenvalue 1000 corresponding to the direction at 45° with side $BC$.

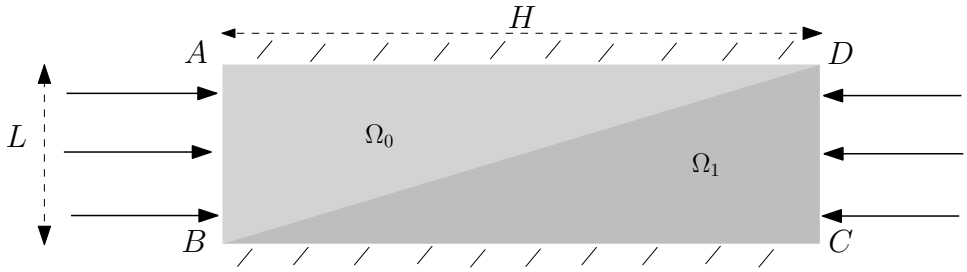


(a)

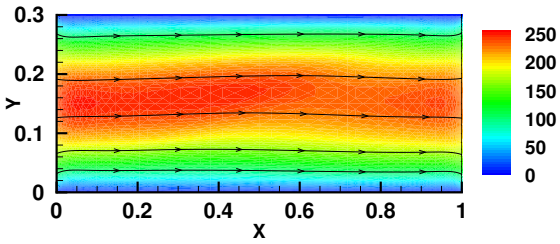


(b) $\bar{\mathbf{\Lambda}}_0(\Omega_1) = \frac{1}{1000}$

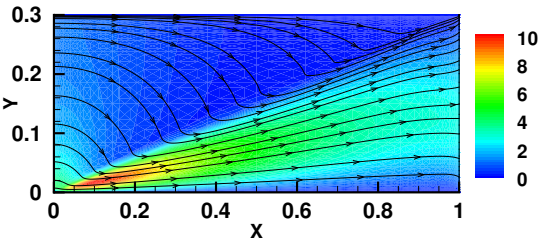


(c) $\bar{\mathbf{\Lambda}}_0(\Omega_1) = 1000$

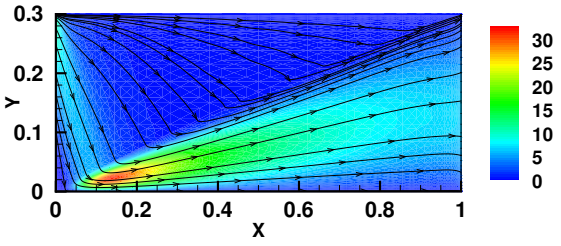


(d) $\bar{\mathbf{\Lambda}}_0(\Omega_1) = 1000$ along $BD$

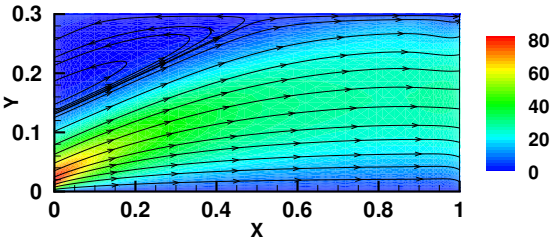


(e) $\bar{\mathbf{\Lambda}}_0(\Omega_1) = 1000$ normal to $BD$

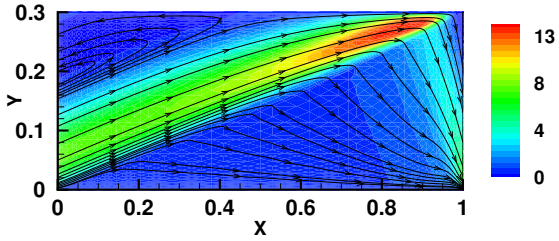


(f) $\bar{\mathbf{\Lambda}}_0(\Omega_0) = 1000$ along $BD$ and $\bar{\mathbf{\Lambda}}_0(\Omega_1) = 1000$ normal to $BD$

Figure 4.3: The streamlines of the flow field and the contours of the velocity component along the flow direction are shown for $\bar{\beta} = 0$. The geometry and arrangement of the inhomogeneous subdomains are also shown.

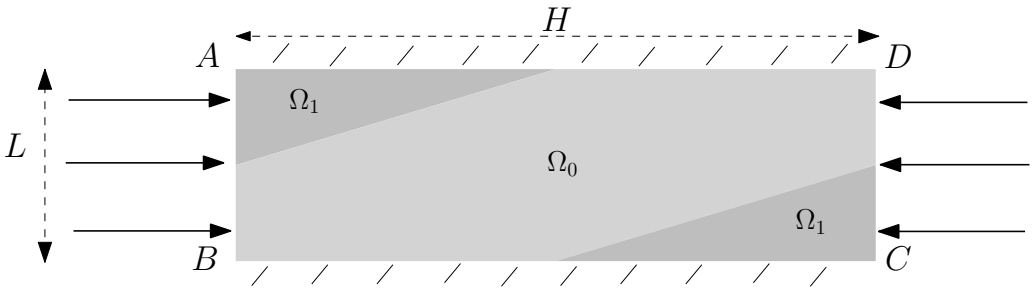


(a)

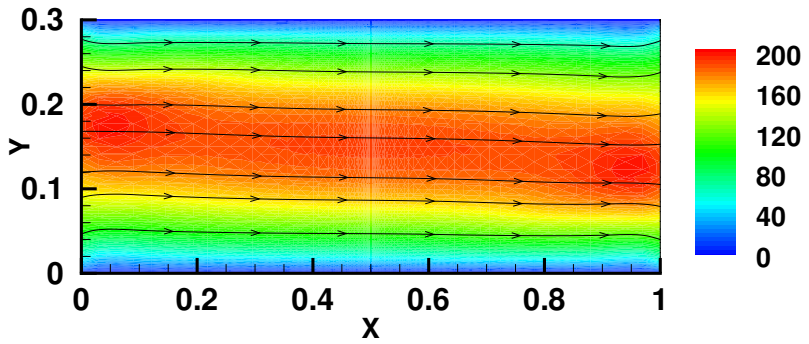


(b) $\bar{\mathbf{\Lambda}}_0(\Omega_1) = \frac{1}{1000}$

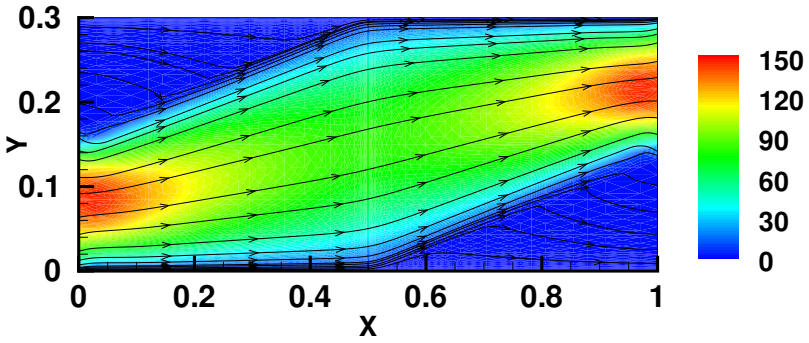


(c) $\bar{\mathbf{\Lambda}}_0(\Omega_1) = 1000$

Figure 4.4: The streamlines of the flow field and the contours of the velocity component along the flow direction are shown for $\bar{\beta} = 0$. As before, the geometry and arrangement of the inhomogeneous subdomains are shown.

# 5. FLOW OF FLUIDS THROUGH POROUS MEDIA DUE TO HIGH PRESSURE GRADIENTS: PART 2 - UNSTEADY FLOWS

Most porous solids are inhomogeneous and anisotropic, and the flows of fluids taking place through such porous solids are inherently unsteady. Such flows have relevance to a wide variety of important technical problems such as the movement of groundwater and contaminants in soils, flow of oil through a reservoir and enhanced oil recovery, carbon dioxide sequestration, diffusion of fluids through synthetic polymers and biological materials, to name a few. Darcy [11] proposed a model in 1856 to study the movement of fluids through porous media which to this day has proven to be the most popular model. However, the model proposed by Darcy does not capture the flow of fluids through porous media when high pressure gradients or flow velocities are involved and in view of this several alternate models have been proposed (see Brinkman [18, 19], Forchheimer [17]). A hierarchy of models for the flow of fluids through porous media can be found in the article by Rajagopal [47].

Darcy's model is based on numerous assumptions (see assumptions (1)-(9) listed earlier in the introduction) and as these premises are not necessarily valid in most technical applications, various modifications have been made to the model in order to account for instance the inertial effects of the fluid, the deformation of the solid, etc. However, most of these modifications are totally ad hoc (Verruijt [76]). An interesting class of applications concerning flow through porous media concerns flows of fluids involving very high pressures and pressure gradients in the flow domain. Examples of such applications are the problems of Enhanced Oil Recovery (EOR) and Carbon dioxide sequestration (COS), wherein the fluid is subject to high pressures and pressure gradients. For such problems, the classical Darcy model and the Brinkman model are grossly inadequate and it is necessary to take into account the fact that both the viscosity of the fluid and the drag coefficient should depend on the pressure, and they both can vary by orders of magnitude in the flow field.

We earlier reviewed the considerable experimental evidence to support the fact that the viscosity of a fluid depends on the pressure. This in turn would imply that the drag coefficient would also depend on the pressure in the fluid. In view of this, Nakshatrala and Rajagopal [58] generalized the model due to Darcy by assuming the drag coefficient to depend upon the pressure. They studied the flow of a fluid within a porous solid due to a pressure gradient and in marked contrast to the classical result they found that the flux through the porous solid achieved an asymptotic value as the driving pressure gradient increased unlike the predictions of the classical Darcy model that the flux has to increase linearly.A rigorous mathematical study of such a model has been carried out by Benardi, Girault and Rajagopal [77].

While Darcy's model takes into account the effect of drag, it ignores the effect of viscosity within the fluid, that is, it ignores the viscous dissipation within the fluid. The study by Shriram, Bonito and Rajagopal [78] redressed this issue and took into account the viscous effects within the fluid by generalizing the model due to Brinkman by allowing the viscosity and the drag coefficient to depend upon the pressure. The study of Shriram, Bonito and Rajagopal [78] was restricted to steady flows, and in keeping with the results of Nakshatrala and Rajagopal [58], they found that the volumetric flux attained a ceiling.

"Steady state" is a mathematical idealization, and all processes in the real world are initial value problems; some of them attain a state that is reasonably close to what could be characterized as "steady state" after a sufficient time interval. When our interest in such processes often lies purely in the long term behaviour, we are content to model the problem as one of "steady state". In other problems however, our interest may squarely lie in the initial transients, or the problem may be such that it may never attain a steady state and in that case the temporal evolution of the problem needs to be considered. In EOR and CS, if we wish to consider flow of a fluid through a *deforming* porous solid, then the inertial effects cannot be neglected. Before getting to that however, it is important to solve the simpler problem of unsteady flow of a fluid through a saturated rigid porous solid. This sets the stage for the problem considered in this paper.

We are interested in the problems of EOR and COS, and since the flow in these problems are inherently unsteady and since the fluid is injected at high pressures, in this study we allow for the possibility that the flow is unsteady and that the viscosity and drag are dependent on the pressure, but we assume that the solid is homogeneous and isotropic. We consider the problem wherein the fluid that enters a slab is pulsatile in nature, about a non-zero mean pressure. Our aim was to determine whether the pulsations would enhance the volumetric flux, a phenomenon that is observed in pulsatile flows in pipes; we however find that this is not the case, that is pulsations in the pressure does not lead to flow enhancement. To our knowledge, this is the first study wherein the unsteady flow of a fluid with pressure dependent viscosity through a porous solid is carried out.

In this section, we extend our previous study of flow through porous media due to high pressure gradients (see Shriram *et al.* [78]) and consider a variant of the problem, namely, the flow of a fluid, initially at rest, through a rigid saturated porous medium wherein the flow is engendered by a pulsatile forcing pressure at one end of the solid while the other end is open to the atmosphere (See Figure 5.1). We consider the case when the forcing pressure varies sinusoidally about a non-zero mean value and compare the volumetric flux with the situation when the fluid is subjected to a constant forcing pressure with magnitude equal to the mean value specified earlier. In some applications, it has been found [79, 80, 81, 82, 83, 84] that the volumetric flux can be enhanced by pulsating the pressure gradient about a mean value. It would be interesting to observe whether a similar effect occurs in case of the flow through a porous medium when the fluid viscosity is considered to be pressure dependent.

The problem of pulsatile flow in rigid tubes with various cross sections has been well studied (see [85, 86]). In the context of porous media, the flow through a rigid porous solid due to a pulsatile pressure gradient is investigated in [87, 88] where the classical Brinkman model is used and exact solutions obtained using a semi-inverse technique; it is assumed that the pipe is infinitely long. The limitation of these studies is that they are inapplicable if the viscosity is a function of the pressure; along the direction of infinite extent the pressure

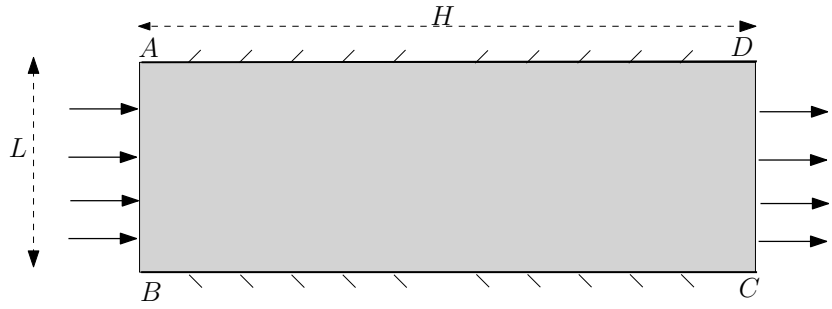


Figure 5.1: Pressure driven flow through a slab of length $L$ and width $H$. A purely normal traction is applied at the left and right boundaries. The fluid satisfies no-slip boundary condition at the top and bottom of the slab. The forcing pressure on the left end varies with time.

becomes unbounded and so does the viscosity. Of course, the notion of an infinite pipe is an idealization in order to simplify the flow field and in all practical problems one deals with a bounded body. Interestingly, this also ensures that the viscosity remains bounded. Our investigation is restricted to the flow of a fluid with pressure dependent viscosity in a finite slab (see Figure 5.1).

The organization of the paper is as follows:In Section 5.1 we introduce the problem and record the governing equations and the boundary conditions. In Section 5.2, we derive the non-dimensional equations that govern the flow, and this is followed by Section 5.3 where we discuss the numerical solution to the problem on hand and make some concluding remarks. A brief description of the finite element scheme used for the computational resolution of the problem is given in Appendix B.

## 5.1 Governing equations

We assume that the liquid is incompressible while the viscosity varies exponentially with the pressure

$$\mu(p) = \mu_0 \exp(\beta p), \quad \mu_0 > 0,\ \beta \geq 0, \tag{5.1}$$

where $\mu_0$ and $\beta$ are constants , with $\mu_0$ having the dimension of viscosity and $\beta$ the dimension that is the inverse of that of the pressure.

Hence the flow of the fluid has to be isochoric and the velocity field must satisfy the constraint that

$$\mathrm{div}[\boldsymbol{v}] = 0. \tag{5.2}$$

The assumption that the viscosity of the fluid depends on the pressure and that the frictional effects in the fluid cannot be ignored implies that the Cauchy stress $\boldsymbol{T}$ in the fluid is given by

$$\boldsymbol{T} = -p\mathbf{1} + 2\mu(p)\boldsymbol{D}, \tag{5.3}$$

where $-p\mathbf{1}$ is the indeterminate part of the stress due to the constraint of incompressibility, $\boldsymbol{v}$ is the velocity of the fluid, $\mu(p)$ is the pressure dependent viscosity and $\boldsymbol{D}$ denotes the symmetric part of the velocity gradient, i.e.,

$$\boldsymbol{D} := \frac{1}{2}\left[\left(\frac{\partial \boldsymbol{v}}{\partial \boldsymbol{x}}\right) + \left(\frac{\partial \boldsymbol{v}}{\partial \boldsymbol{x}}\right)^{T}\right]. \tag{5.4}$$

The balance of linear momentum for the fluid, on neglecting body forces, is given by

$$\rho\frac{d\boldsymbol{v}}{dt} = \mathrm{div}[\boldsymbol{T}] + \boldsymbol{I}, \tag{5.5}$$

where $\boldsymbol{I}$ is the interaction between the solid and the fluid, namely the frictional resistance at the pores of the solid on the fluid that is flowing. It is worth observing that we are only concerned with the balance of linear momentum for the fluid and ignore the balance of linear momentum for the solid as it is assumed to be rigid, the stresses in the solid are what they need to be to guarantee that the balance of linear momentum for the solid is met.

In general, there could be various interaction mechanisms between the flowing fluid and the rigid solid: drag (which is a consequence of the relative velocity between the fluid and the solid), virtual mass effect (a consequence of the relative accelerations of the fluid and the solid), Magnus effect (due to the relative spins of the constituents), Basset forces, Faxen forces, density gradient effects, temperature gradient effects, etc. We shall assume

that the only interaction mechanism is that due to drag and that $\boldsymbol{I}$ is given by

$$\boldsymbol{I} = -\alpha(p)\boldsymbol{v}. \tag{5.6}$$

The "Drag coefficient" is related to the viscosity $\mu$ through $\alpha = \frac{\mu}{k}$ where $k$ is the coefficient of permeability and hence the expression equation (5.1) leads to a "Drag coefficient" $\alpha(p)$ of the form

$$\alpha(p) = \alpha_0 \exp(\beta p), \quad \alpha_0 \geq 0, \tag{5.7}$$

where $\alpha_0$ is a constant with dimension of $\mathrm{ML}^{-3}\mathrm{T}^{-1}$.

Since we shall be interested in slow flow, non-linear terms in the inertial effects in equation (5.5) are neglected.

It follows from equation (5.2)–equation (5.6), on neglecting the convective acceleration term that the appropriate governing equation is

$$-\frac{\partial p}{\partial \boldsymbol{x}} + \mathrm{div}[2\mu(p)\boldsymbol{D}] - \alpha(p)\boldsymbol{v} = \rho\frac{\partial \boldsymbol{v}}{\partial t} \tag{5.8a}$$

$$\mathrm{div}[\boldsymbol{v}] = 0 \tag{5.8b}$$

with initial condition

$$\boldsymbol{v}(\boldsymbol{x}, 0) = \boldsymbol{0} \tag{5.9}$$

We are interested in the flow engendered by application of a pulsatile traction at the left end of the slab while the right end is open to the atmosphere. Due to the applied tractions on the surfaces $AB$ and $CD$, the boundary condition reads

$$\boldsymbol{t}\Big|_{AB} = [-p\mathbf{1} + 2\mu(p)\boldsymbol{D}]\Big|_{AB}\boldsymbol{n}_{AB} = \left[\frac{tF_1}{a}H(a-t) + [F_1 + F_2\sin(\omega(t-a))]\,H(t-a)\right]\boldsymbol{n}_{AB}, \tag{5.10a}$$

$$\boldsymbol{t}\Big|_{CD} = [-p\mathbf{1} + 2\mu(p)\boldsymbol{D}]\Big|_{CD}\boldsymbol{n}_{CD} = p_{\mathrm{atm}}\boldsymbol{n}_{CD}, \tag{5.10b}$$

where

$$H(z) = \begin{cases} 1 \text{ if } z > 0 \\ \frac{1}{2} \text{ if } z = 0 \\ 0 \text{ if } z < 0 \end{cases} \tag{5.11}$$

is the standard Heaviside function.

The expression for the traction has been chosen in order to prevent the impulsive motion of the fluid as it starts from the state of rest; the traction increases linearly from zero and reaches the desired value at time $t = a$.

The fluid obeys the no-slip boundary condition at the other two boundaries:

$$\boldsymbol{v}\Big|_{BC} = \boldsymbol{v}\Big|_{AD} = \mathbf{0}. \tag{5.12}$$

Thus we need to solve equation (5.8) subject to the boundary conditions equation (5.10) , equation (5.12) and the initial condition equation (5.9).

## 5.2 Non-dimensional equations

In order to carry out a systematic study we shall appropriately non-dimensionalize the governing equations. Since the surface $CD$ is exposed to the atmosphere, the mean normal stress is the atmospheric pressure $p_0 = p_{\text{atm}}$. We introduce the following non-dimensionalization

$$\bar{p} := \frac{p}{p_0},\ \bar{\boldsymbol{x}} := \frac{\boldsymbol{x}}{H},\ \bar{\beta} := \frac{\beta}{\frac{1}{p_0}},\ \bar{\boldsymbol{v}} := \frac{\boldsymbol{v}}{v_0},\ \bar{t} := \frac{t}{t_0}, \tag{5.13}$$

where $H$ is the thickness of the slab (see Figure 5.1) and $v_0$ is a representative velocity, say

$$v_0 := \frac{p_0}{\alpha_0 H}. \tag{5.14}$$

while $t_0 := \dfrac{H}{v_0}$ is a representative time. Also, let

$$\bar{\mu} := \frac{\mu}{\mu_0},\ \bar{\alpha} := \frac{\alpha}{\alpha_0}. \tag{5.15}$$

We shall use the following non-dimensional counterpart of equation (5.1)

$$\bar{\mu}(\bar{p}) = \bar{\alpha}(\bar{p}) = \begin{cases} \exp(\bar{\beta}\bar{p}) & \text{if } \bar{p} > 0, \\ 1 & \text{if } \bar{p} \leq 0, \end{cases} \tag{5.16}$$

which is evidently a continuous function of the pressure.

It follows from equation (5.13)–equation (5.16) that equation (5.8) can be expressed as

$$-\bar{\text{grad}}[\bar{p}] - \bar{\alpha}(\bar{p})\bar{\boldsymbol{v}} + \mathcal{A}\bar{\text{div}}[2\bar{\mu}(\bar{p})\bar{\boldsymbol{D}}] = \bar{\rho}\frac{\partial \bar{\boldsymbol{v}}}{\partial \bar{t}}, \tag{5.17a}$$

$$\bar{\text{div}}[\bar{\boldsymbol{v}}] = 0, \tag{5.17b}$$

where $\bar{\text{grad}}[\cdot] := \dfrac{\partial(\cdot)}{\partial \bar{\boldsymbol{x}}}$, $\bar{\text{div}}[\cdot] := \text{tr}[\bar{\text{grad}}[\cdot]]$, $\bar{\boldsymbol{D}} := \dfrac{1}{2}\left[\left(\dfrac{\partial \bar{\boldsymbol{v}}}{\partial \bar{\boldsymbol{x}}}\right) + \left(\dfrac{\partial \bar{\boldsymbol{v}}}{\partial \bar{\boldsymbol{x}}}\right)^T\right]$, $\mathcal{A} := \dfrac{\mu_0}{\alpha_0 H^2}$ is a non-dimensional number that is the ratio of the frictional effect within the fluid due to viscosity to the frictional effect due to drag (friction at pores between the fluid and the solid), $\bar{\rho} := \dfrac{\rho p_0}{(\alpha_0 H)^2}$ is a non-dimensional density. We shall also find it convenient to introduce the additional non-dimensional numbers

$$\gamma := \frac{L}{H}, \quad \bar{\omega} := \frac{\alpha_0 H^2 \omega}{p_0} \quad \bar{F}_1 := \frac{F_1}{p_0}, \quad \bar{F}_2 := \frac{F_2}{p_0}. \tag{5.18}$$

We choose the time instant $t = a$ such that the non-dimensional form of the traction boundary condition is then

$$\bar{\boldsymbol{t}}\Big|_{\bar{x}=1} = -1\mathbf{i}, \tag{5.19a}$$

$$\bar{\boldsymbol{t}}\Big|_{\bar{x}=0} = \left(\bar{t}\bar{F}_1 H(1-\bar{t}) + (\bar{F}_1 + \bar{F}_2 \sin(\bar{\omega}(\bar{t}-1))H(\bar{t}-1)\right)\mathbf{i}, \tag{5.19b}$$

while the corresponding non-dimensional forms for the no-slip boundary condition and initial condition are

$$\bar{\boldsymbol{v}}\Big|_{\bar{y}=0} = \bar{\boldsymbol{v}}\Big|_{\bar{y}=\gamma} = \bar{\boldsymbol{v}}(\bar{\boldsymbol{x}}, 0) = \mathbf{0}. \tag{5.20}$$

The domain and the boundary conditions for equation (5.17) are illustrated in Figure 5.2.

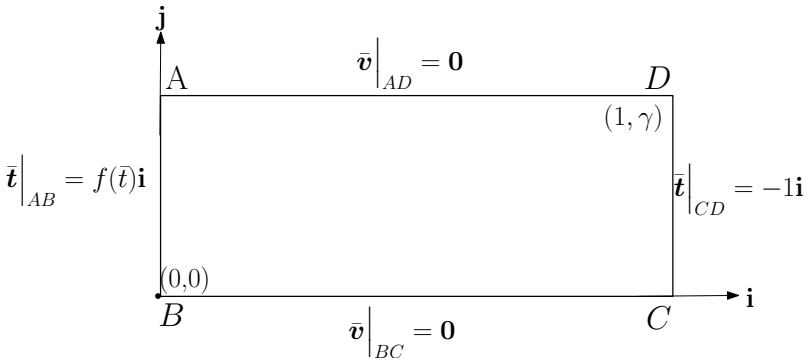


Figure 5.2: Slab of length $\gamma$ and width 1 with boundary conditions indicated on all sides of the slab. The forcing pressure on the left end varies with time.

Thus we solve equation (5.17) with the form for $\bar{\mu}, \bar{\alpha}$ given by equation (5.16) subject to the boundary conditions equation (5.19) and equation (5.20). We postpone to Appendix B the description of the numerical method.

## 5.3 Numerical results

It would be interesting to study the problem for various values of the non-dimensional numbers. Accordingly, we fix $H = 1, \gamma = 0.25, \bar{F}_1 = 300, \bar{F}_2 = 200$ and allow $\mathcal{A}, \bar{\rho}$ and $\bar{\beta}$ to take the values $\mathcal{A} = 0.01,\ 100$, $\bar{\rho} = 1, 10, 100$ and $\bar{\beta} = 0,\ 2 \times 10^{-3}$ and $4 \times 10^{-3}$. Values of $\bar{\beta}$ were chosen from the results of the experiments reported in [45, 46, 44, 43]. We let $\bar{\omega} = \dfrac{\pi}{2}, 0$ in order to compare the response to constant and pulsatile traction.

We shall find it convenient to represent $\bar{\boldsymbol{v}}$ as

$$\bar{\boldsymbol{v}} = \bar{V}_x \mathbf{i} + \bar{V}_y \mathbf{j}. \tag{5.21}$$

The quantity of interest in this problem is the flux or flow rate obtained at the end of the slab that is open to the atmosphere, i.e., the side $CD$. We denote the non-dimensional flux by $\bar{q}$, where

$$\bar{q}(\bar{t}) := \int_{CD} [\bar{\boldsymbol{v}} \cdot \boldsymbol{n}_{CD}] \, \mathrm{d}l = \int_0^{\gamma} \bar{V}_x(1, \bar{y}, \bar{t}) \mathrm{d}\bar{y}. \tag{5.22}$$

We also compute the mean flow rate over one cycle (with time period $\bar{\tau}$) after the initial transients have died down

$$\bar{Q} = \frac{1}{\bar{\tau}} \int_a^{a+\bar{\tau}} \bar{q}(\bar{t}) \mathrm{d}\bar{t} \tag{5.23}$$

and denote the value corresponding to the constant and pulsatile tractions by $\bar{Q}^{\text{const}}$ and $\bar{Q}^{\text{pulse}}$ respectively.

The system of (non-dimensionalized) partial differential equations equation (5.17) with the form for $\bar{\mu}, \bar{\alpha}$ given by equation (5.16) subject to the boundary conditions equation (5.19) and equation (5.20) was solved using a mixed finite element method, details of which are provided in the Appendix B.

From the Figures 5.3–5.7, it can be observed that as the pressure-viscosity coefficient increases, the cumulative volumetric flux obtained upto that instant of time decreases. Moreover, for a given value of $\bar{\rho}$ and $\mathcal{A}$, when one compares the variation of the flux, we see that the cumulative flux is indifferent to the pulsations when $\bar{\beta} = 0$. This is not surprising, since pulsations have no effect on the flow rate for the incompressible Navier-Stokes fluid although for other non-Newtonian fluids [79, 80, 81] the flux does get affected. The trend changes when $\bar{\beta} = 2 \times 10^{-3}, 4 \times 10^{-3}$ and the cumulative volumetric flux for pulsatile traction is lesser than that obtained for constant traction (see Table 5.1). From the table, it can be seen that when $\mathcal{A} = 100$ and the pressure-viscosity coefficient for the fluid is known to be $\bar{\beta} = 4 \times 10^{-3}$, the classical Brinkman model ($\bar{\beta} = 0$) predicts that

pulsating the forcing pressure about a non-zero mean value *would not change* the flow rate while our calculations (using a generalization of the Brinkman model that takes into account the pressure dependence of the viscosity and consequently the drag coefficient) predict a *reduction* of almost 8 % in the flow rate. This suggests that for the flow of such fluids through a porous medium, one cannot increase the volumetric flux by pulsating the pressure about a mean value. The values of the mean flow rate differ both qualitatively and quantitatively, and it makes a compelling case for the use of models that incorporate the pressure dependence of viscosity.

Secondly, one can observe the effects of inertia when the value of $\bar{\rho}$ is increased. The time taken for onset of the long term behaviour is delayed significantly as expected.

Table 5.1: Comparison of the mean flux for constant and pulsatile traction. The percent change in the mean flux relative to $\bar{Q}^{\text{const}}$ is also shown. The pulsations enhance the flow rate when the viscosity is a constant but decrease the flow rate when the fluid viscosity depends on pressure.

| $\mathcal{A}$ | $\bar{\rho}$ | $\bar{\beta}=0$ | | | $\bar{\beta}=2\times10^{-3}$ | | | $\bar{\beta}=4\times10^{-3}$ | | |
|---|---|---|---|---|---|---|---|---|---|---|
| | | $Q^{\text{const}}$ | $Q^{\text{pulse}}$ | % | $Q^{\text{const}}$ | $Q^{\text{pulse}}$ | % | $Q^{\text{const}}$ | $Q^{\text{pulse}}$ | % |
| 0.01 | 1 | 24.33 | 24.33 | 0 | 18.27 | 17.5 | -4.21 | 14.13 | 13.18 | -6.72 |
| 0.01 | 10 | 24.31 | 24.31 | 0 | 18.27 | 18.03 | -1.31 | 14.12 | 13.64 | -3.40 |
| 100 | 1 | 0.004 | 0.004 | 0 | 0.00298 | 0.00284 | -4.70 | 0.00231 | 0.00213 | -7.79 |
| 100 | 10 | 0.004 | 0.004 | 0 | 0.00298 | 0.00284 | -4.70 | 0.00231 | 0.00214 | -7.36 |

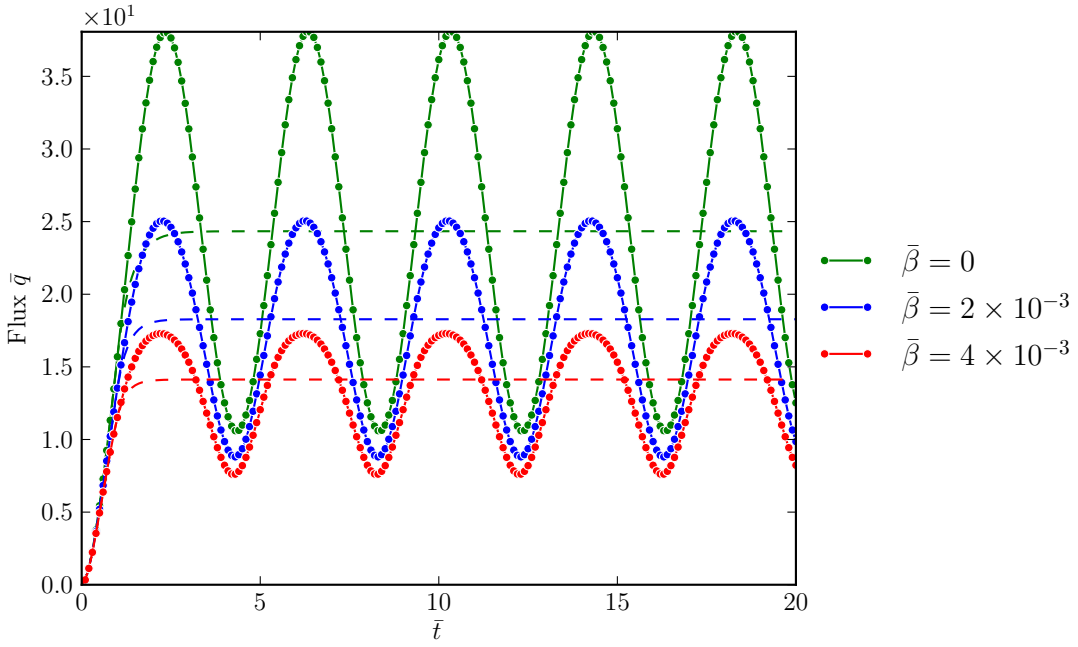


Figure 5.3: Variation of flux with time for $\mathcal{A} = 0.01, \bar{\rho} = 1$ under constant and sinusoidal traction. The dotted lines in the plot denote the flux for constant traction.

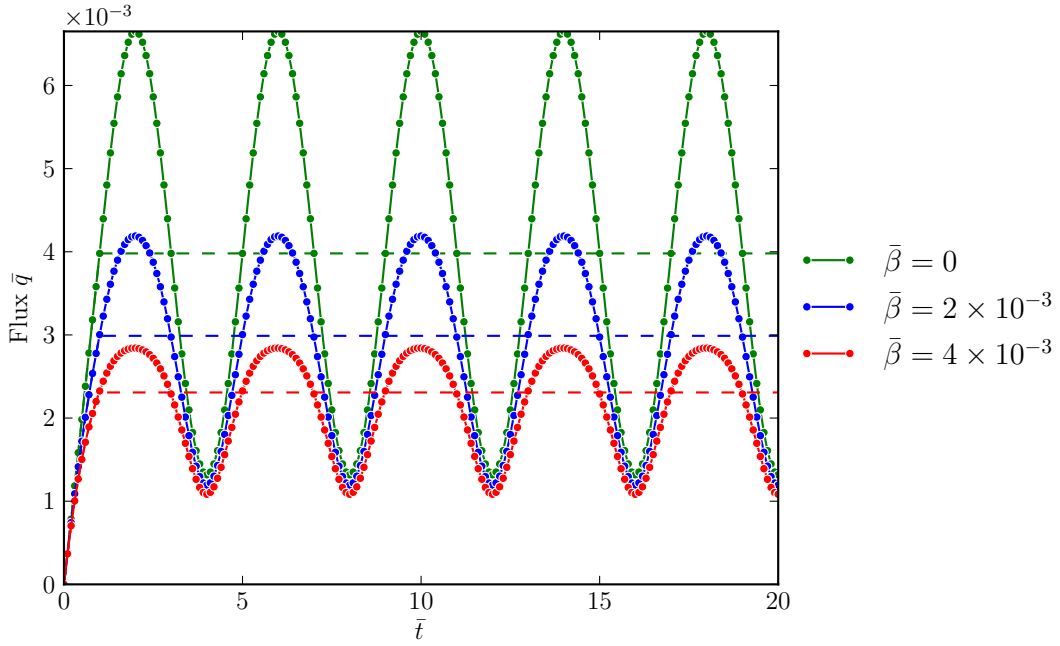


Figure 5.4: Variation of flux with time for $\mathcal{A} = 100, \bar{\rho} = 1$ under constant and sinusoidal traction. The dotted lines in the plot denote the flux for constant traction.

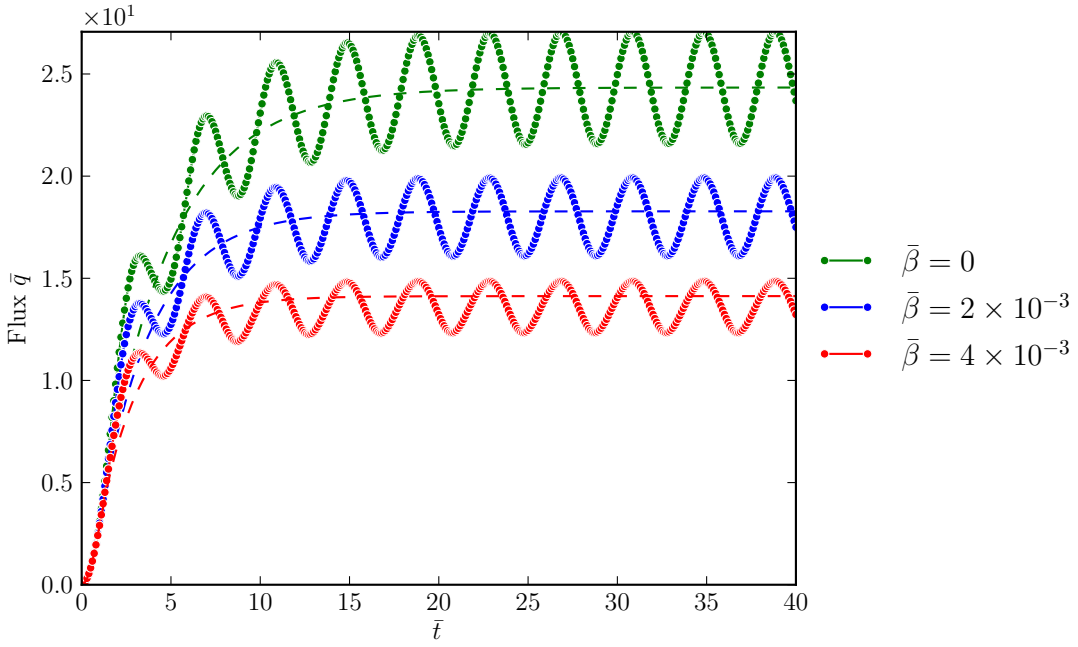


Figure 5.5: Variation of flux with time for $\mathcal{A} = 0.01, \bar{\rho} = 10$ under constant and sinusoidal traction. The dotted lines in the plot denote the flux for constant traction.

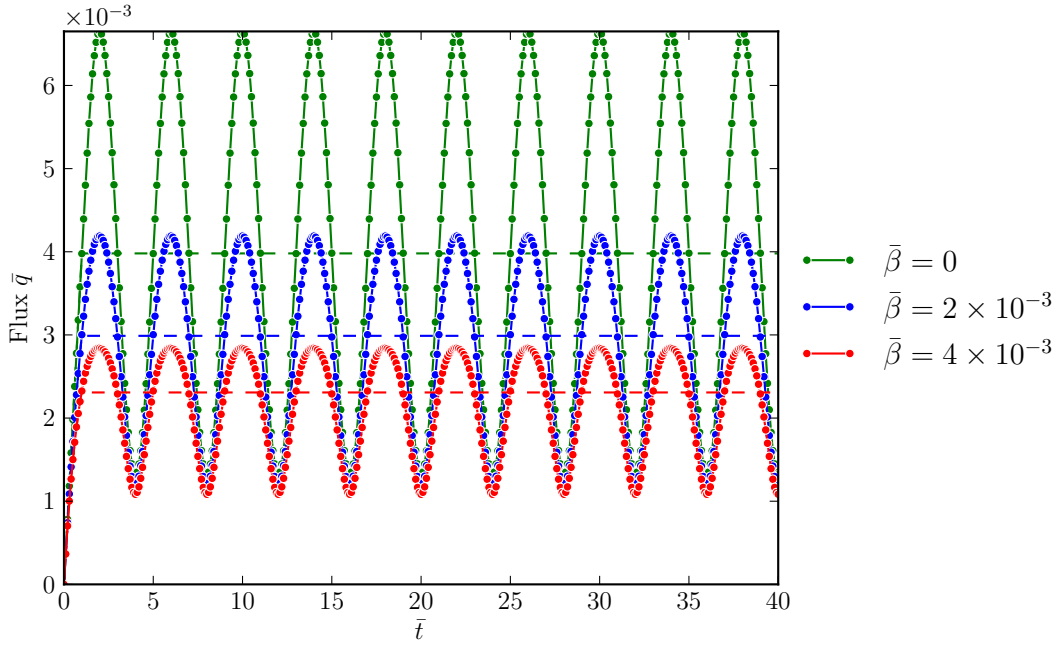


Figure 5.6: Variation of flux with time for $\mathcal{A} = 100, \bar{\rho} = 10$ under constant and sinusoidal traction. The dotted lines in the plot denote the flux for constant traction.

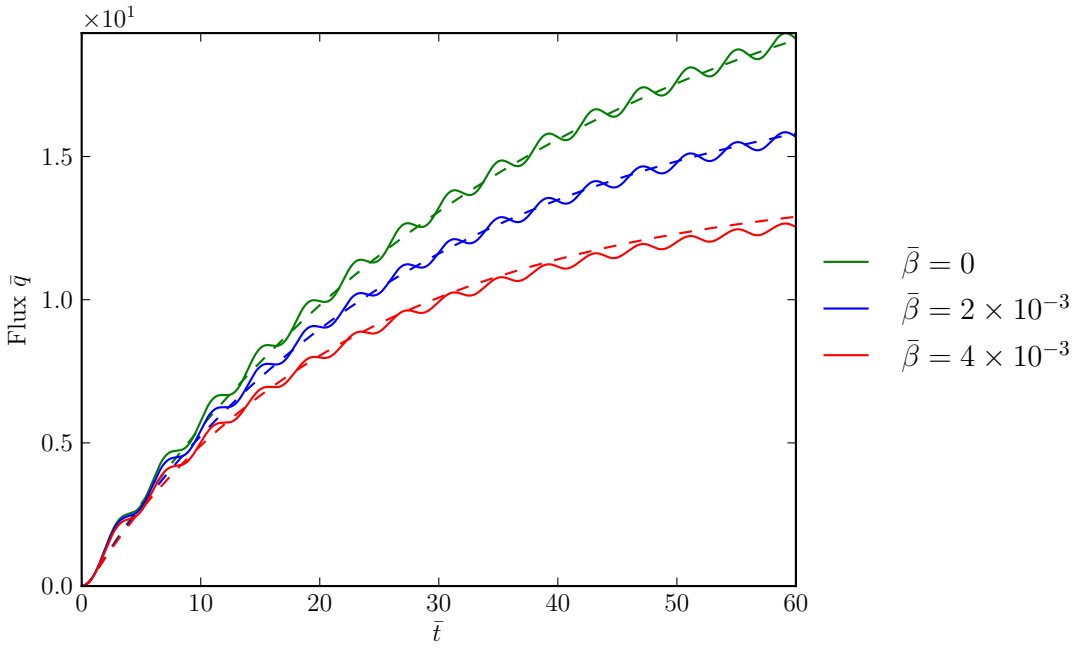


Figure 5.7: Variation of flux with time for $\mathcal{A} = 0.01, \bar{\rho} = 100$ under constant and sinusoidal traction. The dotted lines in the plot denote the flux for constant traction.

# 6. CONCLUSIONS

## 6.1 Concluding remarks

In the problem of flow of a fluid through a porous media due to a large pressure gradient, there are multiple features that need to be taken into account in order to model the process with fidelity. In this dissertation, we focussed on the dependence of the fluid viscosity on the pressure and studied the flow through a porous rigid slab first due to a constant pressure and later a pulsatile pressure (with non-zero mean) applied at the boundary, the former modelled as a steady flow problem while the latter provided a case of unsteady flow. The volumetric flux obtained in the problems departs significantly from that of the case when the viscosity is assumed constant.

Firstly, the results suggest that the flow in the slab is eventually "choked", i.e., as the driving pressure is increased the volumetric flux increases and eventually achieves an asymptotic value. To one unfamiliar with the subject, the result may not appear remarkable; it is the comparison with the standard models in use (none of which incorporate the pressure dependence of viscosity) that makes it so. The classical Brinkman or Darcy models do not predict a ceiling flux, instead they suggest that the volumetric flux can be increased indefinitely by increasing the driving pressure.

Secondly, the results show that the volumetric flux is more for a constant pressure than for a pulsatile pressure with equivalent mean value. This is contrary to what is observed in certain non-Newtonian fluids where the flux is enhanced by the pulsations. If the viscosity is assumed constant, however, there is no difference in the flow rates obtained.

This dissertation makes a cogent argument in favour of models which take into account the pressure dependence of viscosity when studying the flow of fluids through a porous media involving very high pressure differentials, such as enhanced oil recovery or carbon dioxide sequestration.

## 6.2 Suggestions for future work

In the flow of a fluid through a porous solid, one would like to predict all quantities of interest knowing the nature of the mixture constituents (solid and fluid in this case). But this is easier said than done, for the deformation of the solid due to the flow of fluid through it could be highly non-linear, in extreme cases the solid could fracture due to the pressure of the fluid, and the fluid itself may show non-linear behaviour. Being able to accurately describe such situations quantitatively is the ultimate goal.

From the view point of numerical methods, a robust technique that can tackle the exponential variation in the viscosity and "Drag coefficient" with respect to the pressure would be a welcome addition. The boundary value problem considered here was merely a first step in the direction of solving a boundary value problem on a realistic flow domain that corresponds to practical problems.

From the point of view of modeling the physical phenomena associated with enhanced oil recovery or carbon dioxide sequestration, there are multiple issues that need attention. Here we point out possible directions for further work on these problems.

(a) The study on unsteady problems can be extended naturally to account for the convective acceleration terms in the equation which were neglected in this study. The addition of the inertial non-linearity may change the behaviour of the solution.

(b) We do not have a single fluid but rather a mixture of two fluids, say steam and oil in enhanced oil recovery. Thus we need to develop models that can adequately capture the interaction between the constituents. A study similar to this for a mixture of two incompressible fluids would be a noteworthy first step in this direction.

(c) The only interaction between the constituents we considered was the drag. However, in other situations, there are a host of other interaction effects that may become important. In an unsteady flow , for instance, one could consider the virtual mass effect which arises when an object accelerates in a fluid or the Basset force which is a correction to the drag due to the unsteady motion. There can be other interaction effects

due to density or temperature gradients as well. The reader is directed to [89] for a detailed discussion.

(d) The viscosity of the fluid varies with both pressure and temperature. It increases with pressure but decreases with temperature, hence these are competing effects and depending on the process, one may dominate the other. In problems with significant temperature gradients, the effect of temperature cannot be neglected and incorporating it in the model would then mean having to simultaneously solve an additional partial differential equation governing the evolution of temperature.

(e) In general it might be necessary to take into account the fact that the fluid in question is shear thinning. This would lead both the viscosity and the drag coefficient to depend on the shear rate (or to be precise the second principal invariant of the symmetric part of the velocity gradient).

(f) The porous solid in reality is not rigid, it deforms due to the flow of the fluid through it. The deformation of the solid due to the flow of the fluid could be non-linear. As a first approximation one could model the solid as a linearized elastic solid and then study a boundary value problem. Of course the question of appropriate boundary conditions for such problems is of great interest in its own right.

(g) Eventually, one needs to recognize that the high pressure could lead to hydraulic fracture of the solid (a phenomenon known as "fracking" in the petroleum industry which releases oil that was trapped inside the porous solid) which is very important. At this point however, this problem is intractable since the fracture of a single solid by itself poses a stiff challenge.

# REFERENCES


[1] L. W. Lake and P. B. Venuto. A niche for enhanced oil recovery in the 1990s. *Oil & Gas Journal*, 88(17):55–61, 1990.

[2] A.R. Kovscek and M.D. Cakici. Geologic storage of carbon dioxide and enhanced oil recovery. II Cooptimization of storage and recovery. *Energy Conversion and Management*, 46(11–12):1941–1956, 2005.

[3] Philip H. Stauffer, Hari S. Viswanathan, Rajesh J. Pawar, and George D. Guthrie. A system model for geologic sequestration of carbon dioxide. *Environ. Sci. Technol.*, 43(3):565–570, 2008.

[4] Jan Martin Nordbotten, Michael A. Celia, Stefan Bachu, and Helge K. Dahle. Semianalytical solution for $CO_2$ leakage through an abandoned well. *Environ. Sci. Technol.*, 39(2):602–611, 2004.

[5] Anozie Ebigbo, Holger Class, and Rainer Helmig. $CO_2$ leakage through an abandoned well: problem-oriented benchmarks. *Computational Geosciences*, 11(2):103–115, 2007.

[6] E. Lindeberg. Escape of $CO_2$ from aquifers. *Energy Conversion and Management*, 38:S235–S240, 1997.

[7] Jan M. Nordbotten, Dmitri Kavetski, Michael A. Celia, and Stefan Bachu. Model for $CO_2$ leakage including multiple geological layers and multiple leaky wells. *Environ. Sci. Technol.*, 43(3):743–749, 2008.

[8] William G. Gray. A derivation of the equations for multi-phase transport. *Chemical Engineering Science*, 30(2):229–233, 1975.

[9] Majid Hassanizadeh and William G. Gray. General conservation equations for multiphase systems: 1. averaging procedure. *Advances in Water Resources*, 2:131–144, 1979.

[10] In Ulrich Hornung, editor, *Homogenization and Porous Media*, volume 6 of *Interdisciplinary Applied Mathematics*. Springer, New York, 1997.

[11] Henry Darcy. *Les Fontaines Publiques de la Ville de Dijon*. Victor Dalmont, Paris, 1856.

[12] P. A. C. Raats. *Rational Thermodynamics*, chapter Applications of the theory of mixtures in soil physics, Appendix 5D, pages 326–343. Springer, New York, 1984.

[13] D. Munaf, D. Lee, A. S. Wineman, and K. R. Rajagopal. A boundary value problem in groundwater motion analysis-comparisons based on Darcy's law and the continuum theory of mixtures. *Mathematical Modeling and Methods in Applied Science*, 3:231–248, 1993.

[14] F. Cusack, S. Singh, C. Mccarthy, J. Grieco, M. De Rocco, D. Nguyen, H. Lappin-Scott, and J.W. Costerton. Enhanced oil recovery-three-dimensional sandpack simulation of ultramicrobacteria resuscitation in reservoir formation. *Microbiology*, 138(3):647–655, 1992.

[15] S.E. Minkoff, C.M. Stone, S. Bryant, M. Peszynska, and M.F. Wheeler. Coupled fluid flow and geomechanical deformation modeling. *Journal of Petroleum Science and Engineering*, 38(1-2):37–56, 2003.

[16] C.M. Oldenburg, K. Pruess, and S.M. Benson. Process modeling of $CO_2$ injection into natural gas reservoirs for carbon sequestration and enhanced gas recovery. *Energy Fuels*, 15(2):293–298, 2001.

[17] P. Forchheimer. Wasserbewegung durch Boden. *Zeitschrift des Vereines Deutscher Ingeneieure*, 45:1782–1788, 1901.

[18] H. C. Brinkman. On the permeability of the media consisting of closely packed porous particles. *Applied Scientific Research*, A1:81–86, 1947.

[19] H. C. Brinkman. A calculation of the viscous force exerted by a flowing fluid on a dense swarm of particles. *Applied Scientific Research*, A1:27–34, 1947.

[20] M. S. Malashetty, J. C. Umavathi, and J. Prathap Kumar. Two fluid flow and heat transfer in an inclined channel containing porous and fluid layer. *Heat and Mass Transfer*, 40(11):871–876, 2004.

[21] Oleg Iliev and Vsevolod Laptev. On numerical simulation of flow through oil filters. *Computing and Visualization in Science*, 6(2):139–146, 2004.

[22] S. Harris, D. Ingham, and I. Pop. Mixed convection Boundary-Layer flow near the stagnation point on a vertical surface in a porous medium: Brinkman model with slip. *Transport in Porous Media*, 77(2):267–285, 2009.

[23] P. W. Bridgman. *The Physics of High Pressure*. MacMillan Company, New York, USA, 1931.

[24] G. G. Stokes. On the theories of internal friction of fluids in motion and of the equilibrium and motion of elastic solids. *Transactions of Cambridge Philosophical Society*, 8:287–305, 1845.

[25] C. Barus. Isotherms, isopiestics and isometrics relative to viscosity. *American Journal of Science*, 45:87–96, 1893.

[26] M. Paluch, Z. Dendzik, and S. J. Rzoska. Scaling of high-pressure viscosity data in low-molecular-weight glass-forming liquids. *Physical Review B*, 60(5):2979–2982, 1999.

[27] K. L. Johnson and J. L. Tevaarwerk. Shear behavior of elastohydrodynamic oil films. *Proceedings of the Royal Society of London Series A-Mathematical Physical and Engineering Sciences*, 356(1685):215–236, 1977.

[28] K. L. Johnson and J. A. Greenwood. Thermal-analysis of an Eyring fluid in elastohydrodynamic traction. *Wear*, 61(2):353–374, 1980.

[29] K. L. Johnson and R. Cameron. Shear behavior of elastohydrodynamic oil films at high rolling contact pressures. *Proc. Inst. Mech. Eng.*, 182(1):223–229, 1967.

[30] K. R. Harris and S. Bair. Temperature and pressure dependence of the viscosity of diisodecyl phthalate at temperatures between 0 and 100 degrees C and at pressures to 1 GPa. *Journal of Chemical and Engineering Data*, 52(1):272–278, 2007.

[31] E. M. Griest, W. Webb, and R. W. Schiessler. Effect of pressure on viscosity of higher hydrocarbons and their mixtures. *The Journal of Chemical Physics*, 29(4):711–720, 1958.

[32] W. G. Cutler, R. H. McMickle, W. Webb, and R. W. Schiessler. Study of the compressions of several high molecular weight hydrocarbons. *The Journal of Chemical Physics.*, 29(4):727–740, 1958.

[33] R. Casalini and S. Bair. The inflection point in the pressure dependence of viscosity under high pressure: a comprehensive study of the temperature and pressure dependence of the viscosity of propylene carbonate. *The Journal of Chemical Physics*, 128(8):1–7, 2008.

[34] J. T. Bendler, J. J. Fontanella, and M. F. Shlesinger. A new Vogel-like law: ionic conductivity, dialectric relaxation and viscosity near the glass transition. *Physical Review Letters*, 87(19):1–4, 2001.

[35] S. Bair and F. Qureshi. Ordinary shear-thinning and its effect upon EHL film thickness. In D. Dowson et al., editors, *Tribological Research and Design for Engineering Systems*, pages 693–699. Elsevier, Amsterdam, 2003.

[36] S. Bair and P. Kottke. Pressure-viscosity relationships for elastohydrodynamics. *Tribology Transactions*, 46(3):289–295, 2003.

[37] S. Bair, M. Khonsari, and W. O. Winer. High-pressure rheology and limitations of the Reynolds equation. *Tribology International*, 31(10):573–586, 1998.

[38] D. Dowson and G. R. Higginson. *Elastohydrodynamic Lubrication: The Fundamentals of Roller and Gear Lubrication.* Pergamon Press, Oxford, 1966.

[39] K. R. Rajagopal. A semi-inverse problem of flows of fluids with pressure-dependent viscosities. *Inverse Problems in Science and Engineering*, 16(3):269–280, 2008.

[40] E. N. da. C. Andrade. Viscosity of liquids. *Proceedings of the Royal Society of London, Series A*, 215:36–43, 1952.

[41] K. R. Rajagopal. Rethinking the developments of constitutive relations. To appear.

[42] C. J. Schaschke, S. Allio, and E. Holmberg. Viscosity measurement of vegetable oil at high pressure. *Food and Bioproducts Processing*, 84(3):173–178, 2006.

[43] Richard C. Penwell, Roger S. Porter, and Stanley Middleman. Determination of the pressure coefficient and pressure effects in capillary flow. *Journal of Polymer Science Part A-2: Polymer Physics*, 9(4):731–745, 1971.

[44] J. M. Paton and C. J. Schaschke. Viscosity measurement of biodiesel at high pressure with a falling sinker viscometer. *Chemical Engineering Research and Design*, 87(11):1520–1526, 2009.

[45] E. H. Abramson et al. Viscosity of carbon dioxide measured to a pressure of 8 GPa and temperature of 673 k. *Physical Review E*, 80(2):021201, 2009.

[46] V. Vesovic, W. A. Wakeham, G. A. Olchowy, J. V. Sengers, J. T. R. Watson, and J. Millat. The transport properties of carbon dioxide. *Journal of physical and chemical reference data*, 19(3):763–808, 1990.

[47] K. R. Rajagopal. On a hierarchy of approximate models for flows of incompressible fluids through porous solids. *Mathematical Models and Methods in Applied Sciences*, 17:215–252, 2007.

[48] R. J. Atkin and R. E. Craine. Continuum theories of mixtures: Basic theory and historical development. *The Quaterly Journal of Mechanics and Applied Mathematics*, 29:209–244, 1976.

[49] R. J. Atkin and R. E. Craine. Continuum theories of mixtures: Applications. *The Quaterly Journal of Mechanics and Applied Mathematics*, 17:153–207, 1976.

[50] R. M. Bowen. Theory of mixtures. In A. C. Eringen, editor, *Continuum Physics*, volume III. Academic Press, New York, 1976.

[51] A. Fick. Über diffusion. *Poggendorff's Annalen der Physik und Chemie*, 94:59–86, 1855.

[52] C. Truesdell. Sulla basi della thermomechanica. *Rendiconti dei Lincei*, 22:158–166, 1957.

[53] C. Truesdell. Sulla basi della thermomechanica. *Rendiconti dei Lincei*, 22:33–38, 1957.

[54] J.E. Adkins. Non-Linear Diffusion I. Diffusion and Flow of Mixtures of Fluids. *Philosophical Transactions of the Royal Society of London. Series A, Mathematical and Physical Sciences*, 255(1064):607–633, 1963.

[55] J.E. Adkins. Non-Linear Diffusion II. Constitutive Equations for Mixtures of Isotropic Fluids. *Philosophical Transactions of the Royal Society of London. Series A, Mathematical and Physical Sciences*, 255(1064):635–648, 1963.

[56] Ivan Samohyl. *Thermodynamics of Irreversible Processes in Fluid Mixtures*. Teubner, Leipzig, 1987.

[57] K. R. Rajagopal and L. Tao. *Mechanics of Mixtures*. World Scientific Publishing, River Edge, New Jersey, USA, 1995.

[58] K. B. Nakshatrala and K. R. Rajagopal. A numerical study of fluids with pressure dependent viscosity flowing through a rigid porous media. *International Journal for Numerical Methods in Fluids*, 67:342–368, 2009.

[59] K. Kannan and K. R. Rajagopal. Flow through porous media due to high pressure gradients. *Applied Mathematics and Computation*, 199:748–759, 2008.

[60] K. R. Rajagopal and A. R. Srinivasa. A Gibbs-potential-based formulation for obtaining the response functions for a class of viscoelastic materials. *Proceedings of the Royal Society A: Mathematical, Physical and Engineering Science*, 467(2125):39–58, 2011.

[61] K. R. Rajagopal and A. R. Srinivasa. On the thermodynamics of fluids defined by implicit constitutive relations. *Zeitschrift für Angewandte Mathematik und Physik (ZAMP)*, 59(4):715–729, 2008.

[62] K. R. Rajagopal and A. R. Srinivasa. On the thermomechanics of materials that have multiple natural configurations. Part I: Viscoelasticity and classical plasticity. *Zeitschrift für Angewandte Mathematik und Physik (ZAMP)*, 55(5):861–893, 2004.

[63] K. Rajagopal and A. Srinivasa. On the thermomechanics of materials that have multiple natural configurations. Part II: Twinning and solid to solid phase transformation. *Zeitschrift für Angewandte Mathematik und Physik (ZAMP)*, 55(6):1074–1093, 2004.

[64] K. R. Rajagopal and A. R. Srinivasa. On thermomechanical restrictions of continua. *Proceedings of the Royal Society of London. Series A: Mathematical, Physical and Engineering Sciences*, 460(2042):631–651, 2004.

[65] J. Málek and K. R. Rajagopal. A thermodynamic framework for a mixture of two liquids. *Nonlinear Analysis: Real World Applications*, 9(4):1649–1660, 2008.

[66] D. B. Bogy and P. M. Nagdhi. On heat conduction and wave propagation in rigid solids. *Journal of Mathematical Physics*, 11(3):917–923, 1970.

[67] K. R. Rajagopal. Particle free bodies and point free spaces (in press). *International Journal of Engineering Science*, 2013.

[68] J. Málek, Vít Průša, and K. R. Rajagopal. Generalizations of the Navier-Stokes fluid from a new perspective. *International Journal of Engineering Science*, 48(12):1907–1924, 2010.

[69] V. Girault, F. Murat, and A. Salgado. Finite element discretization of Darcy's equations with pressure dependent porosity. *ESAIM: Mathematical Modelling and Numerical Analysis*, 44(6):1155–1191, 2010.

[70] A. Z. Szeri. *Fluid Film Lubrication: Theory and Design*. Cambridge University Press, Cambridge, 1998.

[71] S. C. Subramanian and K. R. Rajagopal. A note on the flow through porous solids at high pressures. *Computers and Mathematics with Applications*, 53:260–275, 2007.

[72] C. Miranda. *Partial differential equations of elliptic type*, volume 370. Springer-Verlag, Berlin, 1970.

[73] Maria Laura Martins-Costa, Rogério M. Saldanha da Gama, and S. Frey. Modeling of a generalized Newtonian flow through channels with permeable wall. *Mechanics Research Communications*, 27(6):707–712, November-December 2000.

[74] Heraldo S. Costa Mattos, Maria Laura Martins-Costa, and Rogério M. Saldanha da Gama. On the modelling of momentum and energy transfer in incompressible mixtures. *International Journal of Non-linear Mechanics*, 30(4):419–431, 1995.

[75] Jacob Bear and Alexander H. D Cheng. *Modelling groundwater flow and contaminant transport*, volume 23 of *Theory and Applications of Transport in Porous Media*. Springer, New York, 2010.

[76] A. Verruijt. *Theory of Groundwater Flow*. Macmillan, London, second edition, 1982.

[77] C. Bernardi, V. Girault, and K.R. Rajagopal. Discretization of an unsteady flow through a porous solid modeled by Darcy's equations. *Mathematical Models and Methods in Applied Sciences*, 18:2087–2123, 2008.

[78] Shriram Srinivasan, Andrea Bonito, and K.R. Rajagopal. Flow of a fluid through a porous solid due to high pressure gradients. *Journal of Porous Media*, 16(3):193–203, March 2013.

[79] H. A. Barnes, P. Townsend, and K. Walters. Flow of non-Newtonian liquids under a varying pressure gradient. *Nature*, 224(5219):585–587, November 1969.

[80] M.F. Edwards, D.A. Nellist, and W.L. Wilkinson. Pulsating flow on non-Newtonian fluids in pipes. *Chemical Engineering Science*, 27(3):545–553, March 1972.

[81] M.F. Edwards, D.A. Nellist, and W.L. Wilkinson. Unsteady, laminar flows of non-Newtonian fluids in pipes. *Chemical Engineering Science*, 27(2):295–306, February 1972.

[82] B. B. Gupta, P. Blanpain, and M. Y. Jaffrin. Permeate flux enhancement by pressure and flow pulsations in microfiltration with mineral membranes. *Journal of Membrane Science*, 70(2–3):257–266, June 1992.

[83] J.A. Howell, R.W. Field, and Dengxi Wu. Yeast cell microfiltration: Flux enhancement in baffled and pulsatile flow systems. *Journal of Membrane Science*, 80(1):59–71, June 1993.

[84] T. Moschandreou and M. Zamir. Heat transfer in a tube with pulsating flow and constant heat flux. *International Journal of Heat and Mass Transfer*, 40(10):2461–2466, July 1997.

[85] M. Zamir. Pulsatile flow in a rigid tube. In *The Physics of Pulsatile Flow*, Biological and Medical Physics, Biomedical Engineering, chapter 4, pages 67–112. Springer, New York, 2000.

[86] M. Haslam and M. Zamir. Pulsatile flow in tubes of elliptic cross sections. *Annals of Biomedical Engineering*, 26(5):780–787, 1998.

[87] A. V. Kuznetsov and A. A. Avramenko. Start-up flow in a channel or pipe occupied by a fluid-saturated porous medium. *Journal of Porous Media*, 12(4):361–367, 2009.

[88] A. Kuznetsov and D. Nield. Forced convection with laminar pulsating flow in a saturated porous channel or tube. *Transport in Porous Media*, 65(3):505–523, 2006.

[89] G. Johnson, M. Massoudi, and K. R. Rajagopal. A review of interaction mechanisms in fluid-solid flows. Technical Report DOE/PETC/TR-90, DE91000941, United States Department of Energy, 1990.

[90] Sheldon Axler. *Linear Algebra Done Right*. Undergraduate Texts in Mathematics. Springer, New York, second edition, 1996.

[91] Peter Chadwick. *Continuum Mechanics: Concise Theory and problems*. Dover Publications, New York, second edition, 1999.

[92] Mark S. Gockenbach. *Understanding and Implementing the Finite Element Method*. Society for Industrial and Applied Mathematics (SIAM), Philadelphia, 2006.

[93] John D. Hunter. Matplotlib: A 2D Graphics Environment. *Computing in Science & Engineering*, 9(3):90–95, May-Jun 2007.

[94] Otfried Schwarzkopf. The Extensible Drawing Editor Ipe. In *Proceedings of the Eleventh Annual Symposium on Computational Geometry*, SCG '95, pages 410–411, New York, NY, USA, 1995. ACM.

[95] Tecplot. *Tecplot 360: User's Manual*. URL: http://www.tecplot.com, Bellevue, Washington, USA, 2011.

[96] F. Brezzi and M. Fortin. *Mixed and Hybrid Finite Element Methods*, volume 15 of *Springer Series in Computational Mathematics*. Springer-Verlag, New York, USA, 1991.

[97] William H. Press, Saul A. Teukolsky, William T. Vetterling, and Brian P. Flannery. *Numerical recipes: The Art of Scientific Computing.* Cambridge University Press, New York, 2007.

# APPENDIX A

## FINITE ELEMENT FORMULATION-1

The references [90, 91] supply the requisite knowledge of linear algebra and continuum mechanics. The mesh data structure used in the computer program was based on the book by Gockenbach [92]. The packages used for creating line drawings, contour plots and figures are [93, 94, 95].

In this section we provide a short description of the finite element scheme that was used to obtain the numerical results for the boundary value problems considered in Section 3 and Section 4.

Let $\Omega \subset \mathbb{R}^d$ be a non-dimensionalized open bounded domain, where $d = 2, 3$ is the number of spatial dimensions. The boundary $\partial\Omega$ is assumed to be Lipschitz continuous and is divided into two complementary parts $\Gamma^v \cap \Gamma^t = \emptyset$ and $\Gamma^v \cup \Gamma^t = \partial\Omega$. The part $\Gamma^v$ is the part of the boundary on which the velocity is prescribed and is assumed to have non-zero measure while $\Gamma^t$ is the part of the boundary on which the traction $\bar{\boldsymbol{t}}$ is imposed.

In order to write equations equation (3.16) in a weaker form suitable for continuous finite element methods, we denote by $L^2(K)$ the space of square integrable function defined over $K = \Omega$ or $K = \Gamma^t$

$$H^1(\Omega)^d := \left\{ \bar{\boldsymbol{v}} \in L^2(\Omega)^d \,\middle|\, \frac{\partial \bar{\boldsymbol{v}}}{\partial \bar{\boldsymbol{x}}_i} \in L^2(\Omega)^d,\ i = 1, ..., d \right\} \text{ and}$$
$$H_0^1(\Omega)^d := \left\{ \bar{\boldsymbol{v}} \in H^1(\Omega)^d \,\middle|\, \bar{\boldsymbol{v}} = 0 \text{ on } \Gamma^v \right\}.$$

We are now in position to write a weak formulation of equation (3.16): Given $\bar{\boldsymbol{t}} \in L^2(\Gamma^t)$, find $\bar{\boldsymbol{v}} \in H_0^1(\Omega)^d$ and $\bar{p} \in L^2(\Omega)$ such that for all $(\boldsymbol{w}, q) \in H_0^1(\Omega)^d \times L^2(\Omega)$

$$\int_\Omega \bar{\alpha}(\bar{p})\bar{\boldsymbol{v}} \cdot \boldsymbol{w} - \int_\Omega \bar{p}\ \bar{\mathrm{div}}[\boldsymbol{w}] + \frac{2}{\mathcal{A}} \int_\Omega \bar{\mu}(\bar{p})\bar{\boldsymbol{D}} \cdot \bar{\mathrm{grad}}[\boldsymbol{w}] - \int_\Omega \bar{\mathrm{div}}[\bar{\boldsymbol{v}}]\ q = \int_{\Gamma^t} \bar{\boldsymbol{t}} \cdot \boldsymbol{w}, \qquad \text{(A.1)}$$

where the " $\cdot$ " denotes the standard inner product for vectors or tensors (that will be clear from the context). A corresponding conforming finite element formulation reads: Given $\bar{\boldsymbol{t}} \in L^2(\Gamma^t)$, find $\bar{\boldsymbol{v}}_h \in \mathcal{V}_h$ and $\bar{p}_h \in \mathcal{Q}_h$ such that for all $(\boldsymbol{w}_h, q_h) \in \mathcal{V}_h \times \mathcal{Q}_h$

$$\int_\Omega \bar{\alpha}(\bar{p}_h)\bar{\boldsymbol{v}}_h \cdot \boldsymbol{w}_h - \int_\Omega \bar{p}_h \, \bar{\mathrm{div}}[\boldsymbol{w}_h] + \frac{2}{\mathcal{A}} \int_\Omega \bar{\mu}(\bar{p}_h)\bar{\boldsymbol{D}}_h \cdot \bar{\mathrm{grad}}[\boldsymbol{w}_h] - \int_\Omega \bar{\mathrm{div}}[\bar{\boldsymbol{v}}_h] \, q_h = \int_{\Gamma^t} \bar{\boldsymbol{t}} \cdot \boldsymbol{w}_h, \quad \text{(A.2)}$$

where $\bar{\boldsymbol{D}}_h := \dfrac{1}{2}\left[\left(\dfrac{\partial \bar{\boldsymbol{v}}_h}{\partial \bar{\boldsymbol{x}}}\right) + \left(\dfrac{\partial \bar{\boldsymbol{v}}_h}{\partial \bar{\boldsymbol{x}}}\right)^T\right]$ while $\mathcal{V}_h$ and $\mathcal{Q}_h$ are finite-dimensional subspaces of $H_0^1(\Omega)^d$ and $L^2(\Omega)$ respectively.

The *inf-sup* or LBB condition constrains the choice of the finite-dimensional spaces $\mathcal{V}_h$ and $\mathcal{Q}_h$ for finite element formulations equation (A.2) to be suitable approximations of equation (A.1). In particular, equal-order interpolation for both pressure and velocity are not suitable (see [96]). Here the so-called *Taylor-Hood* combination is used. That is, after the domain is divided into a number of quadrilaterals when $d = 2$ or hexahedra when $d = 3$, on each element the pressure is approximated by a piecewise linear polynomial in each variable while the velocity is approximated by a piecewise quadratic polynomial in each variable, both approximations being globally continuous.

In this study, the rectangular domain was divided into $4 \times 100$ rectangles where the pressure was computed at the four corner nodes while the velocity was computed at nine nodes (four corners, four midpoints of sides, and the midpoint of diagonals). The mesh was made extremely fine (almost $10^{-11}$) near the top and bottom in order to capture the steep gradients developed due to the boundary condition.

The resulting system of non-linear algebraic equations was solved by using a Newton-Raphson iteration algorithm in conjunction with a line search as outlined in [97]. The solution to $\bar{\beta} = 0$ was provided as an initial guess for $\bar{\beta} = 1 \times 10^{-3}$ and so on until the desired value of $\bar{\beta}$ was reached.

Note that the viscosity $\bar{\mu}$ and drag $\bar{\alpha}$ given by equation (3.15) are continuous but not

differentiable. Hence in our numerical scheme we approximate it by the smooth function [1]

$$\bar{\mu}_h(\bar{p}) := \exp(\bar{\beta}\bar{p}) \cdot \tfrac{1}{2}\left[1 + \tanh\left(\frac{\bar{p}}{10h_{\min}}\right)\right] + 1 \cdot \tfrac{1}{2}\left[1 + \tanh\left(\frac{-\bar{p}}{10h_{\min}}\right)\right] =: \bar{\alpha}_h(\bar{p}) \quad \text{(A.3)}$$

where $h_{\min}$ represents the length of the smallest element in the mesh.

In the limit of mesh refinement, $\lim_{h\to 0} \bar{\mu}_h(\bar{p}) \to \bar{\mu}(\bar{p})$ and $\lim_{h\to 0} \bar{\alpha}_h(\bar{p}) \to \bar{\alpha}(\bar{p})$ where $\bar{\mu}(\bar{p})$ and $\bar{\alpha}(\bar{p})$ are as in equation (3.15), so our approximation is verified to be consistent.

[1] We are motivated by the fact that the Heaviside function $H(x)$ may be realized as the limit of a sequence of smooth functions, namely, $H(x) = \lim_{n\to\infty} \frac{1}{2}[1 + \tanh(nx)] = \lim_{n\to\infty} [1 + \exp(-2nx)]^{-1}$.

# APPENDIX B

## FINITE ELEMENT FORMULATION-2

In this section we provide a short description of the finite element scheme that was used to obtain the numerical results for the boundary value problems considered in Section 5

Let $\Omega \subset \mathbb{R}^d$ be a non-dimensionalized open bounded domain, where $d = 2, 3$ is the number of spatial dimensions. The boundary $\partial\Omega$ is assumed to be Lipschitz continuous and is divided into two complementary parts $\Gamma^v \cap \Gamma^t = \emptyset$ and $\Gamma^v \cup \Gamma^t = \partial\Omega$. The part $\Gamma^v$ is the part of the boundary on which the velocity is prescribed and is assumed to have non-zero measure while $\Gamma^t$ is the part of the boundary on which the traction $\bar{\boldsymbol{t}}$ is imposed.

We discretize the time interval of interest into $N$ instants denoted by $t_n,\ (n = 0, \cdots, N)$. For simplicity, we shall assume uniform time steps, and shall denote the time step by $\Delta t := t_n - t_{n-1}$. However, it should be noted that a straightforward modification can handle non-uniform time steps. We shall denote the time discretized version of a given quantity $z(\boldsymbol{x}, t)$ at the instant of time $t_n$ as follows:

$$z^{(n)} \approx z(\boldsymbol{x}, t_n) \quad n = 0, \cdots, N \tag{B.1}$$

In order to write equations (5.17) in a weaker form suitable for continuous finite element methods, we denote by $L^2(K)$ the space of square integrable function defined over $K = \Omega$ or $K = \Gamma^t$

$$H^1(\Omega)^d := \left\{ \bar{\boldsymbol{v}} \in L^2(\Omega)^d \,\middle|\, \frac{\partial \bar{\boldsymbol{v}}}{\partial \bar{\boldsymbol{x}}_i} \in L^2(\Omega)^d,\ i = 1, ..., d \right\} \text{ and}$$
$$H^1_0(\Omega)^d := \left\{ \bar{\boldsymbol{v}} \in H^1(\Omega)^d \,\middle|\, \bar{\boldsymbol{v}} = 0 \text{ on } \Gamma^v \right\}.$$

We are now in position to write a weak formulation of equation (5.17) after approximating the time derivative by the backward Euler formula, and the viscosity at the current

time instant by using the pressure from the previous time instant:

Given $\bar{\boldsymbol{t}}^{(n+1)} \in L^2(\Gamma^t)$, $\bar{\boldsymbol{v}}^n \in H_0^1(\Omega)^d$ and $\bar{p}^{(n)} \in L^2(\Omega)$ , we need to find $\bar{\boldsymbol{v}}^{(n+1)} \in H_0^1(\Omega)^d$ and $\bar{p}^{(n+1)} \in L^2(\Omega)$ such that for all $(\boldsymbol{w}, q) \in H_0^1(\Omega)^d \times L^2(\Omega)$

$$\begin{aligned}
&\int_\Omega \bar{\rho} \frac{\bar{\boldsymbol{v}}^{(n+1)} - \bar{\boldsymbol{v}}^{(n)}}{\Delta \bar{t}} \cdot \boldsymbol{w} + \int_\Omega \bar{\alpha}(\bar{p}^{(n)}) \bar{\boldsymbol{v}}^{(n+1)} \cdot \boldsymbol{w} - \int_\Omega \bar{p}^{(n+1)} \ \bar{\mathrm{div}}[\boldsymbol{w}] \\
&+ \frac{2}{\mathcal{A}} \int_\Omega \bar{\mu}(\bar{p}^{(n)}) \bar{\boldsymbol{D}}^{(n+1)} \cdot \bar{\mathrm{grad}}[\boldsymbol{w}] - \int_\Omega \bar{\mathrm{div}}[\bar{\boldsymbol{v}}^{(n+1)}] \ q = \int_{\Gamma^t} \bar{\boldsymbol{t}}^{(n+1)} \cdot \boldsymbol{w}, \qquad \text{(B.2)}
\end{aligned}$$

where the " $\cdot$ " denotes the standard inner product for vectors or tensors (that will be clear from the context).

Since the time steps taken are small, we can approximate the viscosity by using the pressure at the previous time instant and this linearizes the partial differential equation and eliminates the possible need for subsequent iterative solution of a non-linear system.

A corresponding conforming finite element formulation reads: Given $\bar{\boldsymbol{t}}^{(n+1)} \in L^2(\Gamma^t)$, $\bar{\boldsymbol{v}}_h^{(n)} \in \mathcal{V}_h$ and $\bar{p}^{(n)} \in \mathcal{Q}_h$, find $\bar{\boldsymbol{v}}_h^{(n+1)} \in \mathcal{V}_h$ and $\bar{p}_h^{(n+1)} \in \mathcal{Q}_h$ such that for all $(\boldsymbol{w}_h, q_h) \in \mathcal{V}_h \times \mathcal{Q}_h$

$$\begin{aligned}
&\int_\Omega \left[ \bar{\alpha}(\bar{p}_h^{(n)}) + \frac{\bar{\rho}}{\Delta \bar{t}} \right] \bar{\boldsymbol{v}}_h^{(n+1)} \cdot \boldsymbol{w}_h - \int_\Omega \bar{p}_h^{(n+1)} \ \bar{\mathrm{div}}[\boldsymbol{w}_h] + \frac{2}{\mathcal{A}} \int_\Omega \bar{\mu}(\bar{p}_h^{(n)}) \bar{\boldsymbol{D}}_h^{(n+1)} \cdot \bar{\mathrm{grad}}[\boldsymbol{w}_h] \\
&- \int_\Omega \bar{\mathrm{div}}[\bar{\boldsymbol{v}}_h^{(n+1)}] \ q_h = \int_{\Gamma^t} \bar{\boldsymbol{t}}^{(n+1)} \cdot \boldsymbol{w}_h + \int_\Omega \frac{\bar{\rho}}{\Delta \bar{t}} \bar{\boldsymbol{v}}_h^{(n)} \cdot \boldsymbol{w}_h, \qquad \text{(B.3)}
\end{aligned}$$

where $\bar{\boldsymbol{D}}_h^{(n+1)} := \frac{1}{2} \left[ \left( \frac{\partial \bar{\boldsymbol{v}}_h^{(n+1)}}{\partial \bar{\boldsymbol{x}}} \right) + \left( \frac{\partial \bar{\boldsymbol{v}}_h^{(n+1)}}{\partial \bar{\boldsymbol{x}}} \right)^T \right]$ while $\mathcal{V}_h$ and $\mathcal{Q}_h$ are finite-dimensional subspaces of $H_0^1(\Omega)^d$ and $L^2(\Omega)$ respectively.

The problem now reduces to a system of linear algebraic equations which can be solved efficiently using standard techniques. Starting with the given initial condition, the solution at the previous time level is provided and solution is advanced in time (by solving the linear system) until the desired final time instant of $T$ was reached.

The *inf-sup* or LBB condition constrains the choice of the finite-dimensional spaces $\mathcal{V}_h$ and $\mathcal{Q}_h$ for finite element formulations equation (B.3) to be suitable approximations

of equation (B.2). In particular, equal-order interpolation for both pressure and velocity is not suitable (see [96]). Here the so-called *Taylor-Hood* combination is used. That is, after the domain is divided into a number of quadrilaterals when $d = 2$ or hexahedra when $d = 3$, on each element the pressure is approximated by a piecewise linear polynomial in each variable while the velocity is approximated by a piecewise quadratic polynomial in each variable, both approximations being globally continuous.

In this study, the rectangular domain was divided into $20 \times 100$ rectangles where the pressure was computed at the four corner nodes while the velocity was computed at nine nodes (four corners, four midpoints of sides, and the midpoint of diagonals). The mesh was made extremely fine (almost $10^{-13}$) near the top and bottom in order to capture the steep gradients developed due to the boundary condition. A time step of magnitude $\Delta\bar{t} = 0.05$ was used in the computation.